Remote sensing-based forest canopy height mapping: some models are useful, but might they provide us with even more insights when combined?

Nikola Besic[1], Nicolas Picard[2], Cédric Vega[1], Jean-Daniel Bontemps[1], Lionel Hertzog[1], Jean-Pierre Renaud[1,3], Fajwel Fogel[4], Martin Schwartz[5], Agnès Pellissier-Tanon[5], Gabriel Destouet[6], Frédéric Mortier[7,8], Milena Planells-Rodriguez[9], and Philippe Ciais[5]

[1]IGN, ENSG, Laboratoire d'inventaire forestier (LIF), 54000 Nancy, France
[2]Groupement d'Intérêt Public (GIP) Ecofor, 75116 Paris, France
[3]Office National des Forêts RDI, 54600 Villers-lès-Nancy, France
[4]Department of Computer Science, École Normale Supérieure, 75230 Paris, France
[5]LSCE/IPSL, CEA-CNRS-UVSQ, Université Paris Saclay, 91191 Gif-sur-Yvette, France
[6]UMR SILVA, INRAE, AgroParisTech, Université de Lorraine, 54280 Champenoux, France
[7]CIRAD, Forêts et Sociétés, 34398 Montpellier, France
[8]Forêts et Sociétés, University of Montpellier, CIRAD, 34090 Montpellier, France
[9]CESBIO, Université de Toulouse, CNES/CNRS/INRAE/IRD/UPS, 31401 Toulouse, France

Correspondence: Nikola Besic (nikola.besic@ign.fr or n.m.besic@gmail.com)

Abstract. The development of high-resolution mapping models for forest attributes, based on remote sensing data combined with machine or deep learning techniques, has become a prominent topic in the field of forest observation and monitoring. This has resulted in the availability of multiple, sometimes conflicting, sources of information, but at face value, it also makes it possible to learn about forest attributes uncertainty through the joint interpretation of multiple models. This article seeks to endorse the latter, by utilizing the Bayesian Model Averaging approach to diagnose and interpret the differences between predictions from different models. The predictions in our case are forest canopy height estimations for metropolitan France arising from five different models. An independent reference dataset, containing four different definitions of forest height (dominant, mean, maximum and Lorey's) was established from around 5 500 plots of the French National Forest Inventory (NFI), distributed across the entire area of interest. In this study, we evaluate models with respect to their probabilities of correctly predicting measurements/estimations at NFI plots, highlighting the spatial variability in respective model probabilities across the study area. We observed significant variability in these probabilities depending on the forest height definition used, implying that the different models inadvertently predict different types of canopy height. We also present the respective inter-model and intra-model variance estimations, enabling us to grasp where the employed models have comparable contributions but contrasted predictions. We show that topography has an important impact on the models spread. Moreover, we observed that the forest stand vertical structure, the dominant tree species and the type of forest ownership systematically emerge as statistically significant factors influencing the model divergences. Finally, we observed that the fitted higher-order mixtures, which enabled the presented analyses, do not necessarily reduce bias or prevent the saturation of predicted heights observed in the individual models.

1 Introduction

The interest in forest observation and monitoring has particularly surged in the recent years, due to the essential role occupied by forests in the energy and ecological transition our societies are undergoing (e.g. Bontemps et al., 2022). Namely, as important carbon sinks and renewable energy sources, forests represent indispensable levers in mitigating the climate crisis, but also very vulnerable ones, along with all the biodiversity they harbor (IPCC, 2021). Being as well challenging distributed targets, relatively inaccessible for in situ measurements at some parts of the globe, their observation and monitoring have mobilized quite a bit of attention from the remote sensing community (Fassnacht et al., 2023).

As in other domains of remote sensing applications (Li et al., 2022), the forest remote sensing research community has witnessed a rapid increase in the utilization of machine learning and deep learning techniques in recent years, also referred throughout the manuscript as artificial intelligence (AI). This has notably led to numerous developments of remote sensing and AI based models for high resolution mapping of the forest canopy height (Potapov et al., 2021; Morin et al., 2022; Ge et al., 2022; Lang et al., 2023; Liu et al., 2023; Schwartz et al., 2024; Tolan et al., 2024; Fayad et al., 2024; Fogel et al., 2024). Many of these approaches involve utilizing spatial or airborne lidar measurements, such as the Global Ecosystem Dynamics Investigation (GEDI) (Dubayah et al., 2020) or Airborne Laser Scanning (ALS) data. These are often complemented by imaging multi-spectral (Sentinel-2, Landsat, Planet, Spot) and sometimes radar (Sentinel-1, Alos) data in order to achieve a wider and/or denser coverage (Coops et al., 2021).

Lidar measurements provide three-dimensional scattering information allowing generally either to reconstruct to a degree the forest stand structure, or at least to estimate its average shape over a certain footprint. They have an outstanding potential for inferring numerous forest attributes (canopy height, wood volume, above-ground biomass etc.) even in cases of relatively complex forest environments (Evans et al., 2006). However, they either often do not have a recurrent acquisition character (e.g. the development of diachronic acquisitions at regional to national scales is at its early ages), or, as it is the case with the GEDI mission, do not provide a continuous spatial coverage (Dubayah et al., 2020; Besic et al., 2024a).

Multi-spectral and radar imagers typically offer wide, recurrent, and spatially continuous coverage of forests. Yet, except for the particular acquisition setups, as the photogrammetry (Irulappa-Pillai-Vijayakumar et al., 2019) or the polarimetric Synthetic Aperture Radar interferometry - PolInSAR (Brigot et al., 2019), they generally do not provide vertically resolved information about the forest stand. Aside from that, they are also prone to a series of non-negligible issues, as for example: the optical signal saturation (Mutanga et al., 2023) or the multiplicity of forest structure properties simultaneously influencing the radar backscattering signal, causing its apparent saturation (Joshi et al., 2017).

There have been numerous attempts within the forest observation community to reconcile the benefits of lidar and imaging measurements, while also mitigating their respective limitations. AI methods have played a significant role in achieving this, by constructing links between the lidar-derived forest attributes, such as canopy height, and broad coverage images. Nevertheless, these remain models and are therefore obviously far from being faultless. Firstly, electromagnetic interactions in remote sensing data cannot theoretically explain all forest attribute variability. Even if they could, the data would still be prone to imperfections from lidar (Roy et al., 2021; Schleich et al., 2023; Tang et al., 2023; Yu et al., 2024) or imaging sources (Teillet et al., 1982;

Joshi et al., 2017; Mutanga et al., 2023), and from modeling choices and parameterizations. Therefore it makes sense that all of these factors combined induce models to struggle to spatio-temporally reproduce a substantial part of the variability of the forest attributes. Similar effects were also observed in other kinds of spatial modeling, either when it comes to resources (Wadoux and Heuvelink, 2023) or ecological modeling (Ploton et al., 2020).

One way to attenuate these effects would be to combine different models in a way which might optimize their joint performances while enabling a comparative evaluation (Hu et al., 2015; Dormann et al., 2018). This can be done in various ways, depending first and foremost on the availability of validation/reference data. If there is no reference data, the most intuitive way to proceed is the simple average or median of models (e.g. Simple Model Averaging), aiming respectively at smoothing predictions among models or at removing dissident predictions. If reference data are available one could think of a more sophisticated way to construct an average, such as weighted model averaging. This could be based on analyzing the model variables (inputs) dynamics i.e. how well it matches with the observed one (Renaud et al., 2022; Besic et al., 2024b), or as it is far more frequently the case, on evaluating models predictions (output). In the latter case, at least in the environmental sciences, we often recur to the Bayesian model averaging (BMA) (Wintle et al., 2003; Li et al., 2008; Gibbons et al., 2008; Picard et al., 2012). The BMA can be perceived as a weighted mean of various predictions, with weights reflecting the performances of different models. Alternatively, it can be viewed as a finite mixture model, estimating the probability that each observation from an independent validation dataset has been generated by one of the models belonging to an ensemble (Raftery et al., 1997; Hoeting et al., 1999; Raftery et al., 2005).

In this article we apply the BMA with the aim of analyzing five selected AI-based models aiming at spatializing the GEDI or ALS estimated canopy height across metropolitan France, using optical multi-spectral and contingently radar data (Lang et al., 2023; Liu et al., 2023; Morin et al., 2023; Potapov et al., 2021; Schwartz et al., 2024). In order to do so we use in situ measurements and estimations from the French National Forest Inventory (NFI) plots as an independent validation dataset. These approximately 5 500 plots enable us to estimate both overall and local weights of selected models based on four different variants of height measurements/estimations: dominant height, mean height, maximum height, and Lorey's height (Duplat and Perrotte, 1982). By involving auxiliary data related to the topography, the dominant tree species, the forest stand vertical structure and the type of the forest ownership, we as well investigate factors influencing the models spread, i.e. where the models have similar weights but contrasted predictions. Finally, we contrast the performance of individual models against the fitted mixtures at the reference measurement sites, allowing us to highlight the advantages and the limitations (some of which have been previously noted in other fields (Bao et al., 2010; Erickson et al., 2012)) while also identifying potential perspectives of the proposed approach.

The article is organized as follows: in Sec. 2 we present the five employed models, while Sec. 3 introduces the NFI reference datasets. Sec 4 contains the detailed description of the used BMA approach. In Sec. 5, we present the results, followed by the corresponding discussion in Sec. 6. Finally, Sec. 7 provides the concluding remarks of the article.
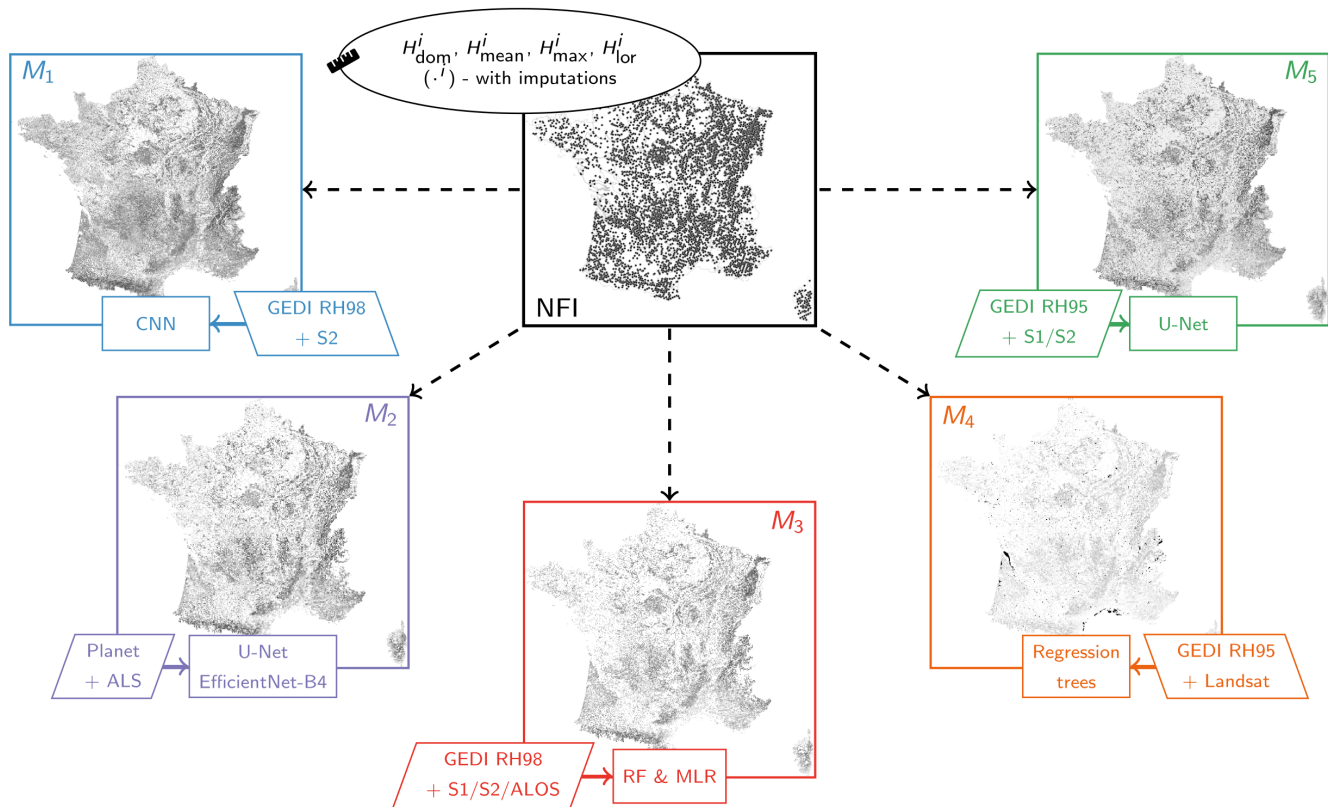
Figure 1. Schematic representation of the Bayesian averaging of the remote sensing-based models for the high resolution mapping of the forest canopy height. NOTE: All the maps are projected in the RGF93 geodetic system with the Lambert-93 projection (EPSG 2154). The rectangles at the bottom of each map indicate the method used, while the parallelograms list the corresponding input datasets. The employed acronyms are defined throughout Sec. 2.

2 Data: Models' descriptions

The selected remote sensing and AI based models differ in terms of the remote sensing data used, but also in the way these data are processed, and in terms of employed AI method. While not the sole commonality among them, a particularly relevant aspect for this study is that they all encompass metropolitan France, where we have access to the reference NFI data. In this section we therefore briefly present their principal characteristics which are partly illustrated in Fig. 1 and will be recalled in sections 5 and 6 while interpreting their mutual differences highlighted by the BMA.

2.1 M_1 (Lang)

The model proposed by Lang et al. (2023) uses Sentinel-2 multi-spectral optical data as input, and aims to spatialize the canopy height estimated from spatially sparse GEDI relative height (RH) profiles. These profiles are derived by averaging lidar

returns across 25 m footprints, depicting the disparity between the elevations of detected ground returns and the $n\%$ cumulative waveform energy, as described in Dubayah et al. (2020). This model uses the 98th percentile of the latter ($n = 98$ - RH98) as a proxy for the canopy height.

The AI method employed is a deep convolutional neural network (CNN) (Lang et al., 2019), taking as input Sentinel-2 spectral bands and geographical coordinates, and producing the canopy height estimate and the associated variance, thanks to the sparse supervision based on the GEDI data. The produced estimates and corresponding variance are spatially resolved at 10 m, refer to the year 2020 (acquisition of GEDI data used as the reference), and cover the entire planet (except for the Arctic and Antarctica).

2.2 M_2 (Liu)

The model crafted by Liu et al. (2023) stands apart in this research as it does not directly utilize GEDI data like the other models. Instead, it obtains its reference data from a range of ALS datasets sourced from different European countries, excluding France. However it indirectly includes the GEDI information through ingesting the previously described Lang et al. (2023) model. The principal modality of this model is the PlanetScope imagery, acquired in the time-frame corresponding to the European late summertime during the year 2019. The 3 m resolution images together with the auxiliary inputs are related to the ALS-derived canopy height using the U-net architecture with an EfficientNet-B4 backbone (Ronneberger et al., 2015; Tan and Le, 2020). The resulting output comprises a map depicting tree cover and canopy height (for areas identified as tree cover), with spatial resolution set at 3 m, spanning the entirety of the European continent. The publicly available product used in this study was however resampled to the spatial resolution of 30 m.

2.3 M_3 (Morin)

Morin et al. (2023) developed a model which uses as predictive variables Sentinel-2 datasets together with Synthetic Aperture Radar (SAR) Sentinel-1 C-band and ALOS-2 PALSAR-2 L-band images. The reference dataset is the canopy height derived from the GEDI data and corresponding to the RH98 metric, adopted as the height reference following a comparison with ALS data. The link between the predictive variables and the reference estimations is built using an algorithm that combines a Random Forest (RF) and a Multiple Linear Regression (MLR), which allows to project the GEDI RH98 measurements onto a 10 m grid covering metropolitan France, for the year 2020.

2.4 M_4 (Potapov)

The Potapov's model (Potapov et al., 2021) depends on the multitemporal metrics derived from Landsat multi-spectral images and reflecting the land surface phenological properties (Potapov et al., 2020). These are used to aliment the bagged regression trees ensemble method (Breiman, 1996), which integrates as well the GEDI RH95 metric-based canopy height estimates. The model output is a global canopy height map for the year 2019, spatially resolved at 30 m.

2.5 M_5 (Schwartz)

125   The model proposed by Schwartz et al. (2024) is based on using Sentinel-2 multi-spectral and Sentinel-1 SAR C-band data. They are integrated, together with the canopy height estimate corresponding to the GEDI RH95 metric, into a U-net model (Ronneberger et al., 2015). The model produces a $10\,\mathrm{m}$ resolution canopy height map covering the metropolitan France for the year 2020.

    Figures A1 and A2 in Appendix A respectively present the mutual comparison of the considered models at the reference
130 measurement sites and representative examples of their estimates in various forestry regions across metropolitan France.

3 Data: Reference dataset description

    National Forest Inventory (NFI) programs are surveys of the forest resources over a certain territory (Tomppo et al., 2010). The French NFI is based on a spatially systematic stratified sampling design, which takes place in two phases: photo-interpretation of around 100k points per year for assessment of forest area, and field observations and measurements at up to
135 $7\,000$ of these points for assessing forest resource variables (Robert et al., 2010; Hervé et al., 2014).

    For each visited point, i.e. plot with a diameter of $25\,\mathrm{m}$, numerous attributes are accessible, including various measurements or estimations of forest canopy height. In this study, we focus on four particular variants among these options:

- H_{dom} – the average tree height of the seven largest trees per plot,

- H_{mean} - the mean tree height,

140   – H_{max} – the maximum tree height.

- H_{lor} – the Lorey's mean tree height - the mean tree height weighted by tree basal area.

    Given that the tree height is measured at the plot only for a sample of trees (one measurement per diameter class and species), complementary values were imputed using a random forest MissForest approach (Stekhoven and Bühlmann, 2012). The method was applied per species and sylvo-ecological region, using the diameter at breast height, the height and the plot
145 level variables (the stem density, the basal area and the wood volume). Validation was done using data acquired during 2005-2009 for which all height measurements were performed. To do so, the current protocol was simulated and imputations were compared with measurements, leading to a mean bias estimate (MBE) of $-0.1\,\mathrm{m}$, a mean absolute error (MAE) of $1.98\,\mathrm{m}$ (14.8%, normalized relative to the target mean value) and a Root Mean Squared Error (RMSE) of $2.66\,\mathrm{m}$ (16.6%, normalized relative to the target mean value).

150   This allows us to have a sample big enough to obtain a potentially better estimate of the height (notably the mean and the dominant one), which are in this case annotated across the manuscript with the superscript i, i.e. H_{dom}^{i}, H_{mean}^{i}, H_{max}^{i} and H_{lor}^{i}.

    In this study, we utilize canopy height estimates from the four variants, sourced from $5\,475$ NFI plots dispersed throughout metropolitan France for the year 2020. All analyses presented in Sec. 5 are based on the supplemented version (estimation -

including imputations), except for the overall weights analysis in Subsec. 5.1, which encompasses both the original version
(measurements - without imputations) and the supplemented version.

4 Method description - a "Bayesian-flavored approach"

Now that we have introduced the five different models and the reference data set, the obvious question would be: which one should we select? The one which compares the best with the reference data? We know that every model, as asserted in the introduction, has its own intrinsic uncertainty. By relying on only one selected model, when many are available, we somehow potentially misjudge the total uncertainty, given that other models could have different predictions with different uncertainties. By applying the BMA method, as introduced in this section, to all available models, we aim to mitigate the above-mentioned issue to some extent (Raftery et al., 2003; Picard et al., 2012), assuming that all models have respectable performance and possess the potential to complement one another. The persistent limitation is that all these uncertainties are assessed at (almost) randomly selected points, namely the NFI plots, leaving the behavior of uncertainty between these points somewhat unpredictable. As will be further elaborated in the manuscript, this limitation also emerges as an important yet motivating challenge. It affects the ability to apply the BMA approach as effectively for synthesizing new spatialized higher-order mixture models as it is for the analysis presented in this study, when relying on sparsely distributed reference datasets.

Here, the BMA assumes combining model outputs without affecting their internal structure (called "the BMA of deterministic models" by Picard et al., 2012). Alternatively, one could also consider employing the BMA for optimizing some of the model parameters simultaneously (known as "the BMA of statistical models" by Picard et al., 2012). While this approach could be relevant for the type of models used in this study, it would first require significant computational resources, as well as a revision of AI-based models to allow certain parameters to remain tunable beyond the training and validation phases.

Let therefore H be the forest canopy height, predicted using the input data $\boldsymbol{x}$, by one of the $K = 5$ considered models, introduced in Sec. 2, denoted as $M_1, \ldots, M_K$. Similarly, let $\mathcal{H}$ denote the reference dataset, introduced in Sec. 3, containing $N = 5\,475$ NFI estimates (referred to as well as the observations across the manuscript). According to the law of total probability we can decompose the posterior distribution of the forest canopy height as:

$$f(H|\mathcal{H}) = \sum_{k=1}^{K} f(H|M_k, \mathcal{H}) \cdot \Pr(M_k|\mathcal{H}), \tag{1}$$

with $f(H|M_k, \mathcal{H})$ being the posterior distribution of the canopy height under model M_k, and $\Pr(M_k|\mathcal{H})$ being the posterior probability of model M_k. The latter sum up to one, and can therefore be somehow interpreted as "importance" weights $(\Pr(M_k|\mathcal{H}) \equiv w_k)$, implying that the posterior distribution of the forest canopy height $f(H|\mathcal{H})$ represents a weighted average of the distributions under participating individual models.

A reasonable assumption when dealing with the canopy height is that its conditional distribution given model M_k can be approximated by a Gaussian distribution centered at the model output m_k:

$$H(\boldsymbol{x})|M_k, \mathcal{H} \sim \mathcal{N}\left(m_k(\boldsymbol{x}), \sigma_k^2\right), \tag{2}$$

with σ_k^2 being the variance of kth model, describing therefore its uncertainty with respect to the $\mathcal{H}$ NFI observation data. Eq. 1 therefore takes the following form:

$$f\left(H(\boldsymbol{x})|\mathcal{H}\right) = \sum_{k=1}^{K} w_k \cdot \phi\left(H; m_k(\boldsymbol{x}), \sigma_k\right), \tag{3}$$

where $\phi(\cdot)$ denotes the Gaussian probability density function. The conditional mathematical expectation of the canopy height can thus be expressed:

$$\mathbb{E}\left(H(\boldsymbol{x})|\mathcal{H}\right) = \sum_{k=1}^{K} w_k \cdot m_k(\boldsymbol{x}), \tag{4}$$

representing essentially the weighted sum of the canopy height predictions of individual models. This comes at the cost of increased complexity, as the mixture involves both the complexity of individual models and the addition of new weights.

Perhaps even more interesting than the mathematical expectation is the variance estimation (Raftery, 1993):

$$\begin{aligned}
\mathrm{Var}\left(H(\boldsymbol{x})|\mathcal{H}\right) &= \sum_{k=1}^{K} w_k \cdot \left(m_k(\boldsymbol{x}) - \sum_{l=1}^{K} w_l \cdot m_l(\boldsymbol{x})\right)^2 \\
&\quad + \sum_{k=1}^{K} w_k \cdot \sigma_k^2,
\end{aligned} \tag{5}$$

which is decomposed into the between-equation variance (first term of Eq. 5) and the within-equation variance (second term of Eq. 5). The former quantifies the models spread i.e. indicates when models have similar weights but contrasted predictions. The latter denotes the weighted average of the individual model uncertainties, reflecting the uncertainty of the ensemble of models, or the total uncertainty outlined at the outset of this section. This implies that the overall uncertainty could be misestimated if only a single model is chosen, even if it performs best in comparison with the reference data.

4.1 E-M algorithm

To compute the expectation (Eq. 4) and the two variances (Eq. 5), we need to derive the weights (w_k) and the standard deviations of the individual models (σ_k). These parameters are estimated from the reference data, which, in this specific context, can be referred to as the training dataset.

If we define the vector of unknown values as:

$$\boldsymbol{\theta} = \left(w_1, \cdots w_K, \sigma_1, \cdots \sigma_K\right), \tag{6}$$

we can formulate the log-likelihood function, allowing to estimate $\boldsymbol{\theta}$ by maximum likelihood:

$$l(\boldsymbol{\theta}) = \sum_{i=1}^{N} \ln\left(\sum_{k=1}^{K} w_k \cdot \phi\left(\mathcal{H}_i; m_k(\boldsymbol{x}_i), \sigma_k\right)\right), \tag{7}$$

where $\mathcal{H}_i$ is the ith observation of dataset $\mathcal{H}$, and $\mathbf{x}_i$ are the input data corresponding to the ith reference height observation.

This cannot be done in closed form, but rather has to be addressed numerically - with the "Expectation-Maximization" (EM) iterative method (Dempster et al., 1977; McLachlan and Krishnan, 2008). This method addresses the problem by introducing the "missing data" z_{ki} which represent the posterior probability that the model k is the one that "fits" the best the observation i. Acknowledging the Bayesian framework underlying this method, which also exhibits some degree of frequentist characteristics (as suggested by Dormann et al., 2018), we refer to it as the "Bayesian-flavored approach".

Starting from the initial guess for $\boldsymbol{\theta}$ ($w_1 = w_2 = \cdots = w_K = 1/K$, $\sigma_1 = \sigma_2 = \cdots = \sigma_K = 1$), in the first - expectation step we compute the missing values for the next step (j) based on the current estimate of the standard deviations ($\sigma_k^{(j-1)}$), and evidently by including the models height estimates ($m_k(\boldsymbol{x}_i)$) and the reference NFI observations ($\mathcal{H}_i$):

$$\hat{z}_{ki}^{(j)} = \frac{\phi\left(\mathcal{H}_i; m_k(\boldsymbol{x}_i), \sigma_k^{(j-1)}\right)}{\sum_{l=1}^{K} \phi\left(\mathcal{H}_i; m_l(\boldsymbol{x}_i), \sigma_l^{(j-1)}\right)}. \tag{8}$$

It is relevant to note that Picard et al. (2012) provide a version of Eq. 8 containing the weight values (w_k) both in the numerator and denominator, and that the one we finally opted for (without weights) comes from Raftery et al. (2003). The reasoning behind this, which is not without significance for the context of the presented work, will be elaborated in Sec. 6.

Once we are done with the expectation step, in the second - maximization step, we can "update" the overall weights:

$$w_k^{(j)} = \frac{1}{N} \sum_{i=1}^{N} \hat{z}_{ki}^{(j)}, \tag{9}$$

as well as the standard deviations:

$$\sigma_k^{(j)} = \sqrt{\frac{\sum_{i=1}^{N} \hat{z}_{ki}^{(j)} \left(\mathcal{H}_i - m_k(\boldsymbol{x}_i)\right)^2}{\sum_{i=1}^{N} \hat{z}_{ki}^{(j)}}}. \tag{10}$$

The iteration continues until the following condition is satisfied:

$$\|\boldsymbol{\theta}^{(j)} - \boldsymbol{\theta}^{(j-1)}\|_1 < 10^{-6}, \tag{11}$$

in which case we have reached the convergence.

5 Results and analysis

Once applied on the models and the NFI data from Sec. 2 and 3, the method introduced in the previous section gives therefore the overall weights of each model across the entire territory of interest (w_k), as well as the local weights at every observation site i - corresponding to the converged "final" value of the "missing data" (z_{ki}). The former is analyzed in Subsec. 5.1, while the latter is being addressed in Subsec. 5.2. The variances estimations (Var$(H(\boldsymbol{x})|\mathcal{H})$) can as well be expressed in the overall or local fashion, the latter being the subject of Subsec. 5.3 and 5.4. The local estimation of the Var$(H(\boldsymbol{x})|\mathcal{H})$, at the point i, is obtained by substituting the weights w_k and w_l in Eq. 5 with the respective "missing data" (z_{ki} and z_{li}).

Since not all models share the same spatial resolution (M_1, M_3 and M_5 at 10 m, while M_2 and M_4 at 30 m), instead of upscaling M_1, M_3 and M_5 to 30 m, we opted to downscale M_2 and M_4 to 10 m. This was achieved by subdividing a 30 m pixel into nine identical ones.
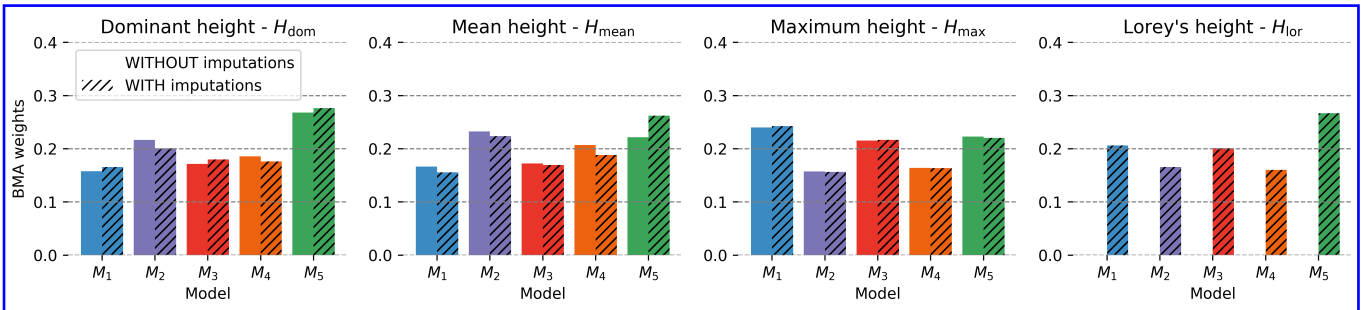
Figure 2. BMA overall weights of M_1 (Lang), M_2 (Liu), M_3 (Morin), M_4 (Potapov) and M_5 (Schwartz) with respect to: (a) the NFI dominant height, (b) the NFI mean height, (c) the NFI maximum height, (d) the NFI mean Lorey's height. As suggested in the legend, different patterns correspond to the presence or the absence of the imputations complementing the NFI measurements, except for the mean Loray's height whose calculation was only possible with the imputations.

5.1 Overall weights

240   Illustrated in Fig. 2, the overall weights allow deducing the following:

- All models contributed to the finite mixtures at the scale of metropolitan France, with the individual weights (w_k) differing relatively significantly from $\frac{1}{5}$, which would be the weight of every model in case of the Simple Model Averaging (SMA). The SMA used here is based on the mean estimate.

- The distribution of contributions changed importantly as a function of the employed height reference (H_{dom}, H_{mean}, 245 H_{max} or H_{lor}). For instance, we can see that the model developed by Schwartz et al. (2024) (M_5) is the most likely to have generated the dominant height measurements/estimations as well as the Lorey's mean height estimations at the NFI plots. We can also notice that the model of Lang et al. (2023) (M_1) slightly outperforms the one of Morin et al. (2023) (M_3) and the model proposed by Schwartz et al. (2024) (M_5) when it comes to the probability to have generated the maximum height measurements/estimations at the NFI plots. This appears to be related to the fact that Lang et al. (2023) 250   and Morin et al. (2023) have chosen the GEDI RH98 metric as an input modality, as opposed to the GEDI RH95 metric retained by M_4 and M_5.

- The inclusion or exclusion of external MissForest imputations in the reference observations significantly influenced the distribution of weights. This effect is particularly obvious when analyzing dominant and mean height, where the introduction of imputations alters the dominant model, i.e., the one with the highest probability of generating the mean 255   height observations, from the model proposed by Liu et al. (2023) (M_2) to M_5.
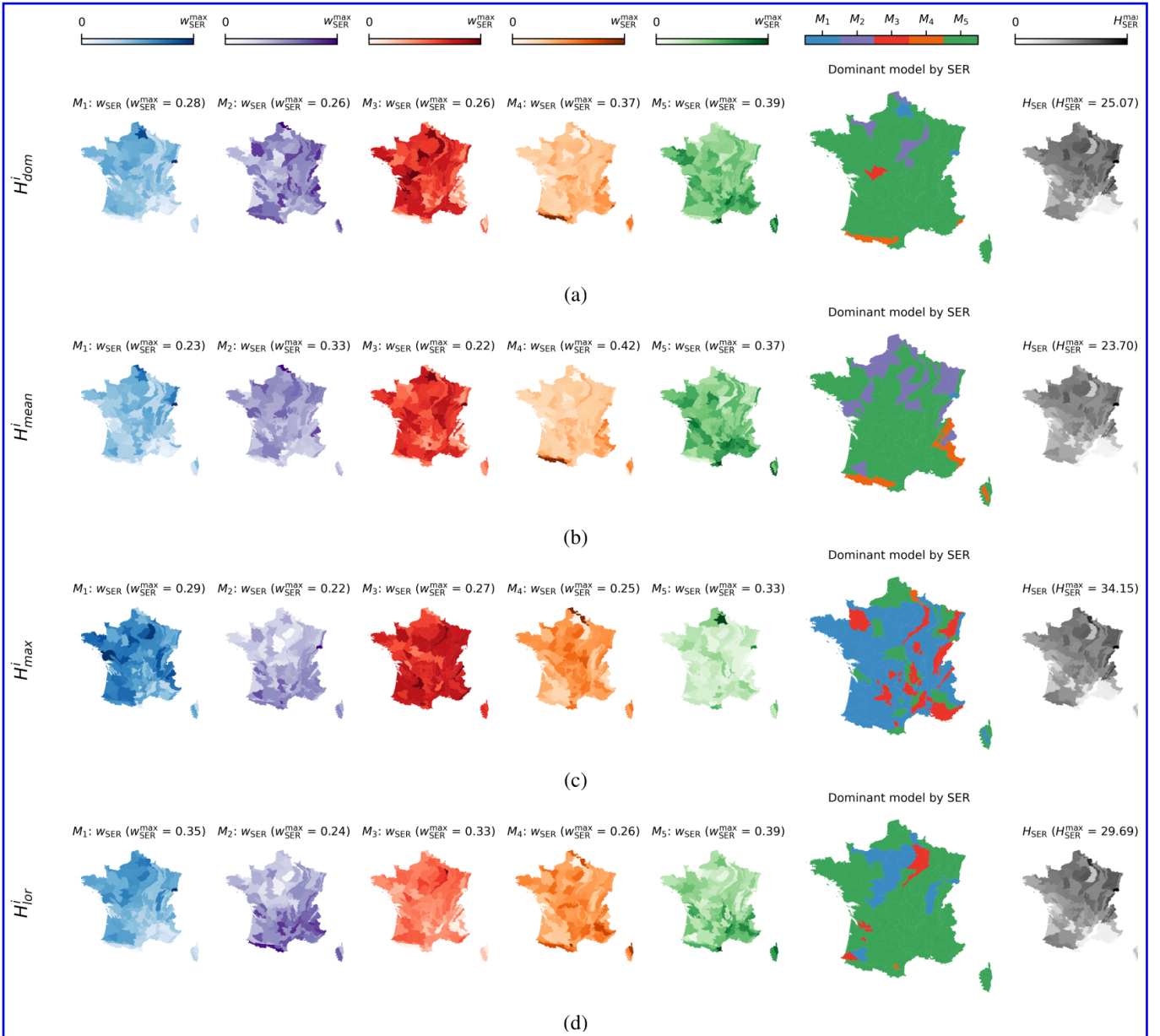
Figure 3. BMA local (regional) weights of M_1 (Lang), M_2 (Liu), M_3 (Morin), M_4 (Potapov) and M_5 (Schwartz) with respect to: (a) the NFI H_{dom}^i, (b) the NFI H_{mean}^i, (c) the NFI H_{max}^i, (d) the NFI H_{lor}^i. Different shades of colors represent variations of regional weights averaged by sylvo-eco region, ranging from 0 to the maximum value of the regional weight indicated in the panel title ($w_{\mathrm{SER}}^{\mathrm{max}}$). The rightmost column represent the average height per sylvo-ecological region derived from the field measurements/estimations.

5.2 Local (regional) weights

The local weights, originally derived at the $5\,475$ NFI plots, were further averaged by sylvo-ecological regions (SER). Namely, metropolitan France is split into 91 of these regions, out of which the 86 non-alluvial, representing a certain homogeneity in terms of sylvo-ecological indicators. This territorial organization is suitable for illustrating local weights, as it would be rather impractical to display them individually.

Illustrated in Fig. 3, the local weights allow the following observations:

- The weights of each model exhibited significant variation across the studied territory, regardless of the variant of reference observations (dominant, mean, maximum, or Lorey's height).

- Though the dominance of different models as a function of the observation height type stated in the previous section remains obvious even after the scale-decomposition (M_5 for H_{dom}^i, H_{mean}^i and H_{lor}^i, while M_1 for H_{max}^i), they were not prevalent in all SERs. That is to say, the model proposed by Potapov et al. (2021), which does not prevail at the overall scale for any of the reference datasets employed, appeared nevertheless to be very performing in perhaps the most challenging SERs in terms of topography (the Alps and the Pyrenees mountain chains, as well as Corsica), for H_{mean}^i, and to a degree, for H_{dom}^i. This can potentially be explained by the spatial resolution of this model based on the Landsat data (30 m), which somehow smooths the adverse effects that mountainous terrain has on most of imaging remote sensing sensors (Riano et al., 2003). We can as well notice that despite the dominance of M_1, models M_3 and M_5 prevail in a pretty important part of the studied territory when it comes to predicting the maximum height. While it's not unexpected for M_3 to exhibit this behavior, as it utilizes the GEDI RH98 metric, it's intriguing to note the same trend in M_5, which employs the GEDI RH95 metric. This observation possibly underscores the influence of C-band SAR data, which should be more sensitive to maximum height rather than other height references.

- Given that height can serve as a proxy for volume/biomass, and recognizing that forests denser in terms of biomass can be more challenging to monitor via remote sensing, we also present in Fig. 3 the average height values by SER. However, this analysis did not reveal any significant impact of average height values by SER on the weight distribution between models, suggesting either that density is not critical enough in temperate forests, or that none of the models stands out in addressing it.

5.3 Influence of topography on the spread

Perhaps the most interesting output of the BMA algorithm in terms of analysis is the variance $\mathrm{Var}\left(H(\boldsymbol{x})|\mathcal{H}\right)$, which is in this subsection decomposed locally into the within-equation (within-variance) and the between-equation (between-variance) one, and averaged by sylvo-ecological regions in an equivalent manner and for the same reasons, as the local weights in the previous subsection. As a reminder, the within-variance indicates the estimated uncertainty of the fitted mixture model, while the between-variance reflects the spread among the models that comprise the mixture.

Figure 4, particularly its left part illustrating locally varying within and between variances for different types of reference observations, enabled us to infer the following:

- The within variance exhibited reasonably consistent values across space, without dramatic spatial variations. The mixtures derived based on H_{dom}^i and H_{lor}^i, where M_5 predominates, displayed the lowest within variance. Notably, this variance was also the least spatially variable among all the considered variants.

- The between variance showed unmistakable patterns - high values in the high-mountainous regions: the Alps and the Pyrenees. It is the case for all variants. This inference is further supported by the analysis presented in the right part of Figure 4, which includes the comparison of between-variance and averaged elevation and slope across sylvo-ecological regions. These values were derived by sampling the $5\,\mathrm{m}$ Digital Terrain Model (DTM) (Institut national de l'information géographique et forestière, 2024a) at the locations of reference observations. The Pearson coefficient of correlation reaches up to 0.69 for the average elevation (H_{max}^i) and up to 0.68 for the average slope (H_{max}^i).

- The within variance consistently exceeded the between variance, indicating that the obtained prediction could be deemed reliable, particularly when considering ensemble learning principles (Mo et al., 2023). An exceeding between variance would have indicated that the models are structurally too different from each other, making their combination ineffective. In such a case, the assumption stated at the beginning of Sec. 4, that the considered models have the potential to complement each other, would have been disproved.

5.4 Influence of categorical variables on the between model spread

In this subsection, we utilized the following categorical variables available at the NFI observation locations (obtained from the NFI database):

- the tree type - broad-leaved vs. coniferous,

- the dominant tree species - selected among some 70 species,

- the forest stand vertical structure - a qualitative observation distinguishing between: temporarily cleared, regular low forest, other regular low stands, irregular vertical structure, regular high with understorey, regular high without understorey, and open woodland structure.

- and the type of forest ownership - having four classes: managed private forest, unmanaged private forest, national (public) forest or any other public forest.

We investigated whether these categorical variables influence the between-variance i.e. the models spread, by applying the analysis of variance (ANOVA) (Kaufmann and Schering, 2014). Table 1 contain the outputs of the ANOVA experiment and allow us to deduce the following:
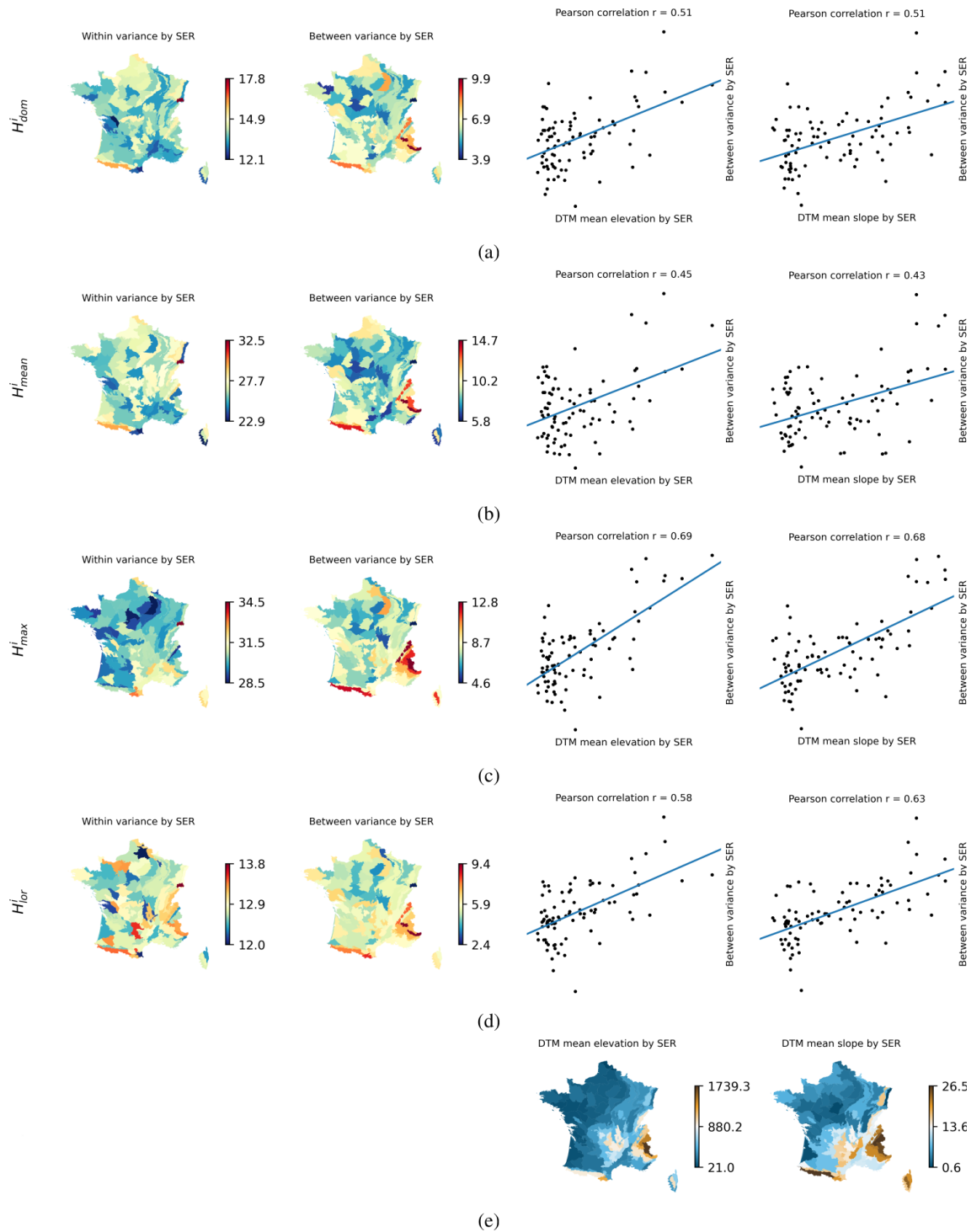
Figure 4. The within variance, the between variance and the comparison between the latter and the DTM mean elevation and slope (e), with the reference being: (a) the NFI H_{dom}^i, (b) the NFI H_{mean}^i, (c) the NFI H_{max}^i, (d) the NFI H_{lor}^i. Blue lines represent the fitted regressions.

Variable	Dom. tree type	Dom. tree species	Vertical structure	Type of forest own.	Residual
Degrees of freedom	1	50	4	3	5302
H_{dom}^{i} — Sum of sq.	0.74	3029.0	2329.1	188.94	122212.5
H_{dom}^{i} — F value	0.03	2.63	25.26	2.73	/
H_{dom}^{i} — **PR$(> F)$**	**0.86**	**< 0.001**	**< 0.001**	**< 0.05**	/
H_{mean}^{i} — Sum of sq.	0	8844.6	4466.3	873.7	255092.9
H_{mean}^{i} — F value	0	3.68	23.2	6.1	/
H_{mean}^{i} — **PR$(> F)$**	**0.99**	**< 0.001**	**< 0.001**	**< 0.001**	/
H_{max}^{i} — Sum of sq.	146.4	6079.5	6336.6	520.7	147335.4
H_{max}^{i} — F value	5.27	4.38	57.01	6.25	/
H_{max}^{i} — **PR$(> F)$**	**< 0.05**	**< 0.001**	**< 0.001**	**< 0.001**	/
H_{lor}^{i} — Sum of sq.	50.3	2754.2	1280.7	242.0	79967.6
H_{lor}^{i} — F value	3.33	3.65	21.23	5.35	/
H_{lor}^{i} — **PR$(> F)$**	**0.07**	**< 0.001**	**< 0.001**	**< 0.05**	/

Table 1. ANOVA: Investigating if the dominant tree type (broad-leaved or coniferous), the dominant tree species, the vertical structure and the type of forest ownership represent statistical significant factors influencing the BMA between variance across different variants of NFI reference.

- The dominant tree type did not consistently emerge as a significant factor influencing the models spread, despite reports from both (Morin et al., 2023) and Schwartz et al. (2024) indicating better performance over coniferous forests than broad-leaved ones. While it appeared to be a significant factor at the $\alpha = 0.05$ significance level for H_{max}^{i}, this significance is not observed for the other variants.

- The dominant tree species consistently emerged as a significant factor influencing the spread of the models at the $\alpha = 0.05$ significance level. Upon examining Fig. B1, we observed that classes such as "other native broad-leaved," European hop-hornbeam (*Ostrya carpinifolia*), or European larch (*Larix decidua*) tend to dominate in causing variations between the models across different reference variants.

- The vertical structure of forest stand also significantly influenced the spread (at the $\alpha = 0.05$ significance level) for all reference observation variants. Fig. B1 indicates that classes such as regular low forest, other regular low stands, and

irregular vertical structures tend to display higher between-variance values compared to classes like regular high with understorey and regular high without understorey.

 – Lastly, the type of forest ownership also had a statistically significant impact on whether the considered models diverge or not. According to the statistics shown in Fig. B1, unmanaged private forests are characterized by the highest between-variance values.

5.5   Fitted mixtures

In this subsection, we contrast the performances of individual models against the fitted mixtures, obtained by substituting the weights w_k in Eq. 4 with the local weights z_{ki}, at the reference measurement sites. We do so by focusing on standard statistical metrics such as coefficient of determination (R^2), mean bias estimates (MBE), and normalized root mean square error ($NRMSE$), the later being normalized with respect to the mean reference value.

Fig. 5 confirms that for each of the four definitions of forest canopy height, the BMA was able to fit a higher-order mixture model that outperforms any individual model and the SMA in terms of R^2 and $NRMSE$. This validates the models' effective complementarity and reinforces the relevance of the analysis in the previous subsections, which primarily explored the spatial variability of the local weights in relation to the employed reference height type.

In order to reinforce the legitimacy of the local weights, we reorganized the exercise from Fig. 5 into a 5-fold cross-validation. Specifically, rather than using all points, only 80% of randomly selected points (Wadoux et al., 2021; Meyer and Pebesma, 2022) were used to derive the local weights. This process was repeated 5 times, with a different quarter of points renewed each time. Each reference dataset is therefore characterized by 4 different estimates of local weights. In Fig. 6, we illustrate the coefficient of variation (CV) between these estimates, averaged by SER for clarity. The observed low values of the CV demonstrate the robustness and representativeness of the estimated local weights, which form the foundation of the analyses presented in the paper. The findings from the test data (20% of randomly selected points) allow us to discuss the interpolation/extrapolation properties of the BMA approach and address the uncertainty between the reference data sites, which will be covered in the following section.

Finally, we as well compared the variance results of the applied BMA to those obtained by the SMA. The latter are obtained if we substitute in Eq. 5 the weights w_k and w_l by the $w = \frac{1}{K} = \frac{1}{5}$, and keep the numerical estimations for the standard deviations σ_k.

Figure 7 depicts the comparison between BMA and SMA in terms of the differences in within and between variances (within - between) for the various variants of reference observations. The results indicate that unlike BMA, where the within-between variance, as observed in Subsection 5.3, consistently remains positive, in the case of SMA, the spread exceeds the variance of the mixture in mountainous regions. This confirms once more that unlike SMA, BMA effectively mixes the considered models (Mo et al., 2023).
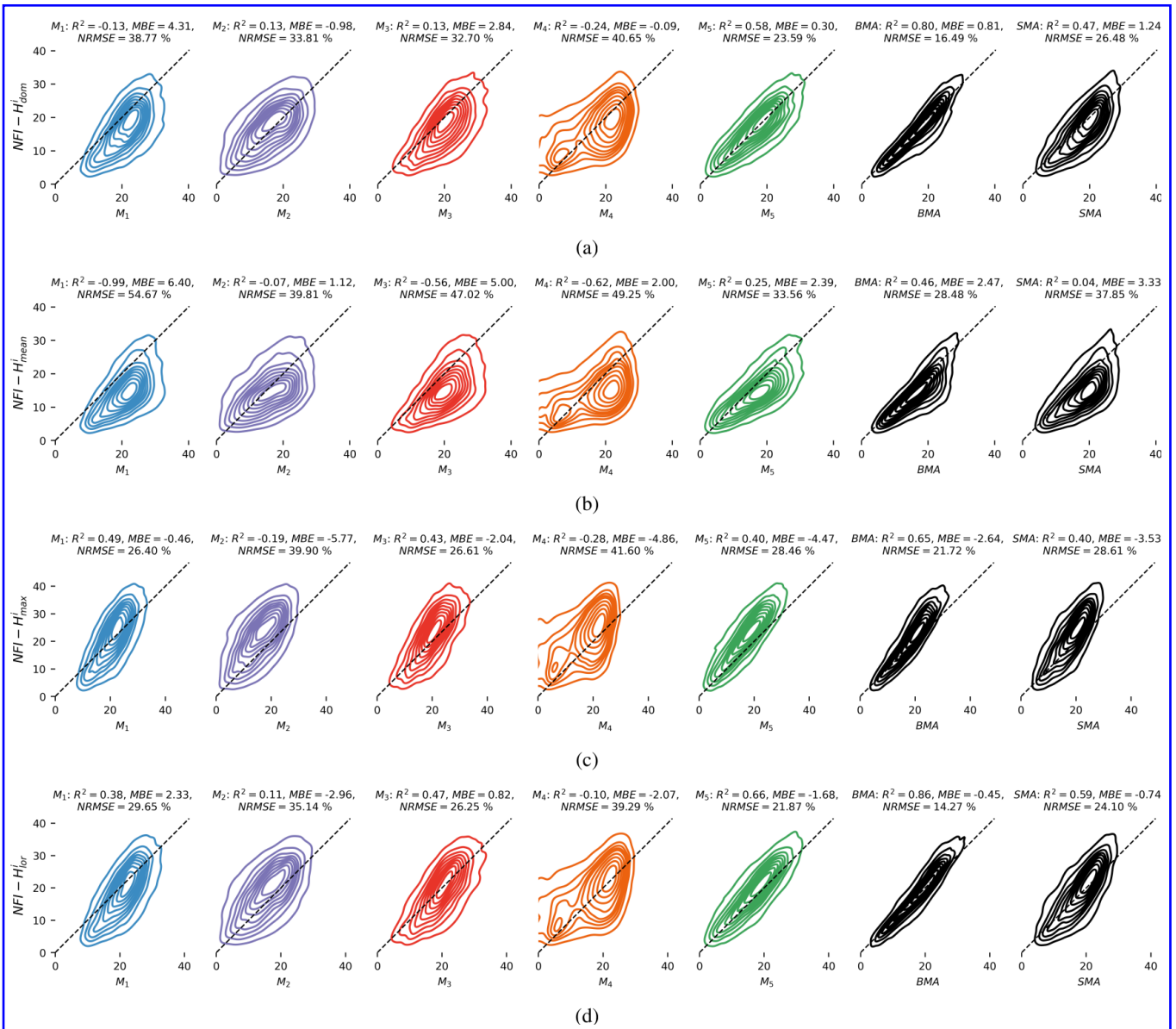
Figure 5. Kernel density estimate (KDE) plots comparing individual models and their BMAs with the four employed NFI references: (a) H_{dom}^i, (b) H_{mean}^i, (c) H_{max}^i, (d) H_{lor}^i.
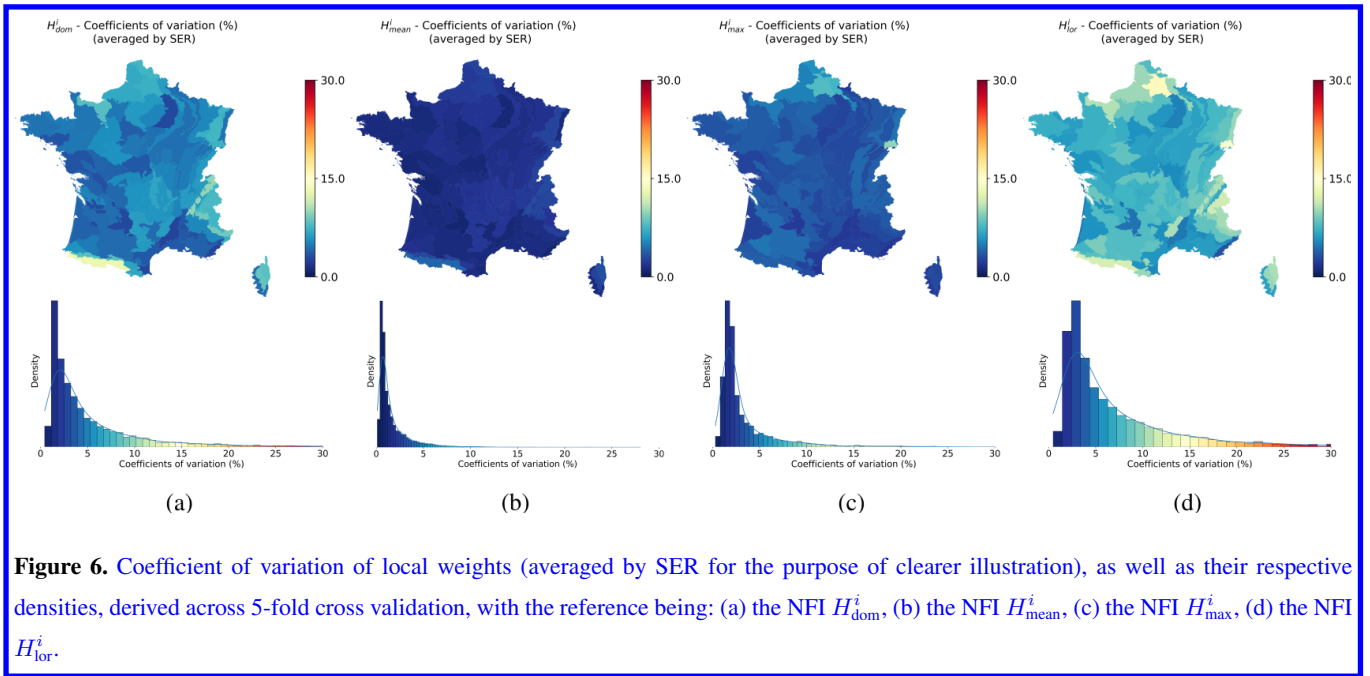
Figure 6. Coefficient of variation of local weights (averaged by SER for the purpose of clearer illustration), as well as their respective densities, derived across 5-fold cross validation, with the reference being: (a) the NFI H_{dom}^i, (b) the NFI H_{mean}^i, (c) the NFI H_{max}^i, (d) the NFI H_{lor}^i.
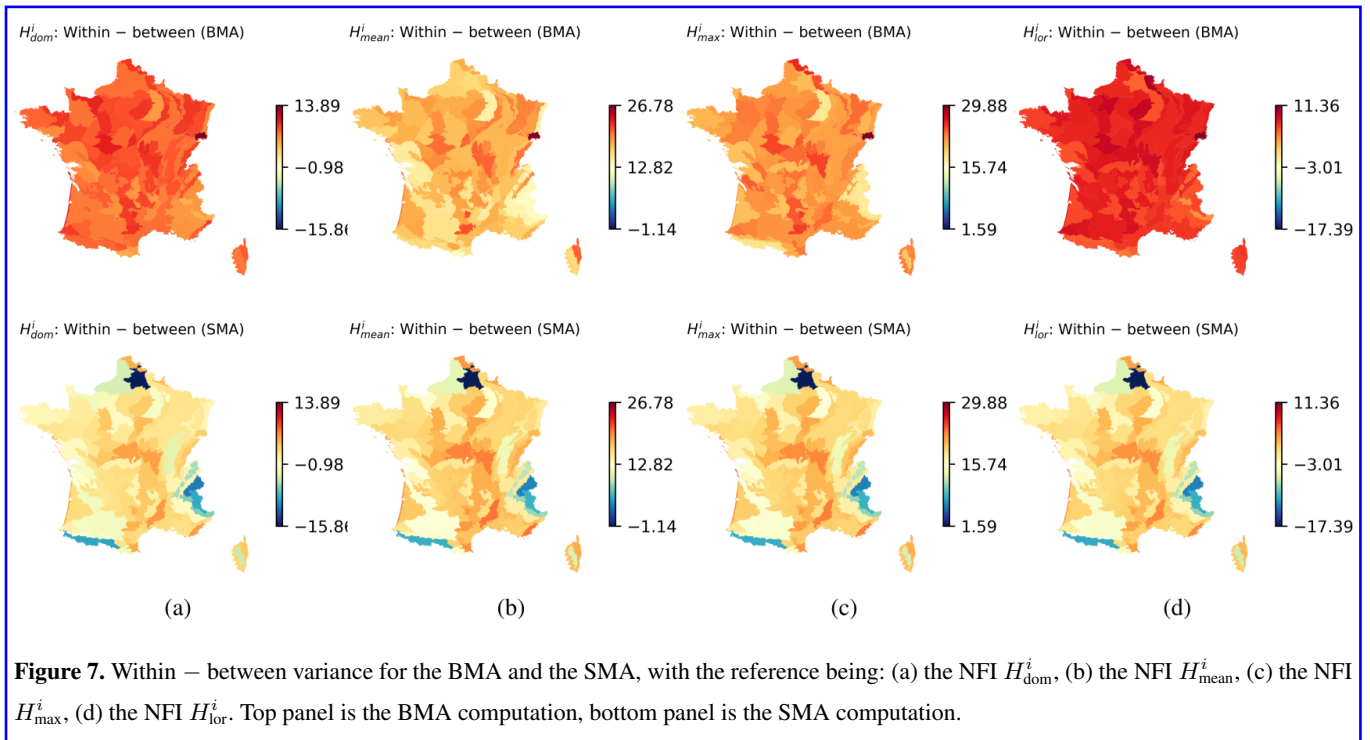
Figure 7. Within − between variance for the BMA and the SMA, with the reference being: (a) the NFI H_{dom}^i, (b) the NFI H_{mean}^i, (c) the NFI H_{max}^i, (d) the NFI H_{lor}^i. Top panel is the BMA computation, bottom panel is the SMA computation.

6 Discussion

The findings outlined in subsection 5.1 indicate that the various models inadvertently tend to predominantly predict different types of forest canopy height. This could indeed be a significant finding for the community, as describing forests with high spatial precision in terms of four canopy height definitions instead of just one could have positive implications for allometric estimations of wood volume or aboveground biomass. Namely, instead of relying on only one allometric relation, one could simultaneously rely on four of them, not differing only in terms of parametrisations (Picard et al., 2012) but also in terms of input variables (a type of height) (Tran-Ha et al., 2011).

This very first portion of the results demonstrated the relatively strong impact of complementing the NFI height measurements/estimations by the missForest imputations, which may prompt consideration of the potential benefits of incorporating this approach into the NFI sampling design, prior to stratified inference.

The findings outlined in subsection 5.2 imply that the fusion of remote sensing-based observational models may need to be scale-dependent, indicating that the contributions of different models vary depending on the focal spatial scale. This aligns closely with a similar message conveyed by Besic et al. (2024b) regarding predictive forest species distribution models.

The results in subsection 5.3 pointed out that the models considered in this study diverge, i.e. have similar weights but contrasted predictions in mountainous terrain. Even though the between-variance remained below the level of the within one, and the mixture was therefore nevertheless reliable even in the mountains, this implies worse performances of the models in mountain environments, which are more challenging (Stage and Salas, 2007). The hypothesis we formulate is that this comes mostly from the quality of remote sensing data, which is lower in mountainous regions, be it from lidar sensors, multi-spectral imagers, or radar sensors. The list of reasons for the latter is long, with the most prominent effects being:

- Mountainous terrain introduces distortions in remote sensing images, particularly due to shadows and slope effects, a phenomenon accentuated in radar data by shadows, layovers, and foreshortenings (Teillet et al., 1982; Moreira et al., 2013). The GEDI data, in particular, are significantly impacted by steep areas, as the distortions of backscattered waveforms within a 25 m footprint introduce additional uncertainty into derived RH profiles (Fayad et al., 2021; Quirós et al., 2021).

- Atmospheric Disturbances - atmospheric conditions such as cloud cover, hydrometeors, and aerosols can affect the quality of remote sensing data (particularly optical sensors), especially in mountainous regions characterized by variable weather patterns and a higher probability of convection events (Vanonckelen et al., 2013).

- Higher heterogeneity - mountainous areas often exhibit diverse vegetation types and land cover classes, which can complicate the job for both remote-sensing based classification and estimation methods (Vanonckelen et al., 2013).

Thus, we pinpoint (high) mountainous regions as an important challenge for ongoing model advancements, particularly since studies like Waser et al. (2021) demonstrate that a combination of Sentinel-1/Sentinel-2, along with Digital Terrain Models (DTMs), can enhance performance in mountainous areas, at least concerning tree type classification (broad-leaved vs.

coniferous). Many well-preserved forest areas worldwide are located in mountainous terrain due to accessibility issues, which makes this particularly important.

The findings exposed in subsection 5.4 suggest that any information about the three out of four considered categorical variables (dominant tree species, vertical structure of forest stand, type of forest ownership) could potentially be a useful modality for the remote-sensing based models for the high resolution mapping of the forest canopy height.

The tree species and the topography impacts (Subsec. 5.3) are undoubtedly mixed, due to the altitudinal zonation, suggesting that tree species can potentially be perceived as a predictor of the variation caused by topographic effects, or vice versa.

An interesting influence of the forest stand vertical structure on the estimation of the canopy height can be explained by the remote sensing signal sensitivity on the entirety of the forest stand scanned. This is obviously the case for the lidar, but appears to be also the case for the radar (Imhoff, 1995), as well as for the optical sensors which can be used to detect and are therefore sensitive to the understory presence/composition (Yang et al., 2023). Discrepancies among models appear to be greater for regular low forests, other low stands, or irregular structures, compared to regular high stands (Fig. B1). This is not surprising, as low structures tend to be more heterogeneous. As a result, they are poorly captured by models that target a specific height proxy. This effect could potentially be reinforced by the fact that all models exhibit some degree of saturation (Fig. 5). Therefore, in contrast to lower heights, the models tend to 'converge' in the case of higher stands, which cannot exactly be corrected by fitting a higher-order mixture model.

While there are no pristine forests in metropolitan France, not all forests are managed to the same extent, and this often depends on ownership type, making it a strong proxy for forest stand complexity (Ehbrecht et al., 2017). The impact of ownership type is likely linked to the previously discussed influence of forest stand vertical structure. For instance, lightly managed private forests, where we observed the highest between-variance, show greater structural variability (26% of low or irregular stands compared to 17% for public forests, or only 30% of regular high stands without understorey). This is a result of public policies and the tendency of large private properties (which are managed) to prioritize large-dimension timber production. This contrasts with currently lightly managed or unmanaged private properties, which have been managed in the past under some form of the coppice system (Hawes, 1908). Moreover, the between-variance increases as unmanaged private forests account for between 55% and 60% of the forested area in metropolitan France, naturally covering the widest observation gradients.

Beyond demonstrating that for each of the four forest canopy height definitions, the BMA successfully fits a mixture that surpasses any individual model and the SMA in terms of R^2 and $NRMSE$, the results shown in subsection 5.5 indicate that the mean bias estimates (MBE) for the mixtures are not lower than those of any of the individual models included. This aligns with the conclusions reported by Bao et al. (2010) and Erickson et al. (2012), suggesting that while BMA effectively addresses variance, it may need to be supplemented with bias correction methods to ensure that the finite mixture not only exhibits significantly reduced variance compared to the participating models but also lower bias. One alternative approach that might yield less biased mixtures, and is worth exploring, would be to adapt the well established employed E-M algorithm by incorporating Restricted Maximum Likelihood Estimation (REML) instead of Maximum Likelihood Estimation (MLE) (Pinheiro and Bates, 2000).

The 5-fold cross-validation confirmed the stability of the estimated local weights, demonstrating a certain competence in predicting the appropriate weights despite changes in the composition of the reference data. An intriguing auxiliary observation worth mentioning in the discussion is that H_{dom}^i and H_{lor}^i seem to exhibit the most sensitivity in terms of weight variability (Fig. 6). This could be because these forest height types heavily depend on diameter distribution, order statistics, or weighted mean, and therefore represent local population properties, unlike H_{max}^i and H_{mean}^i.

Equally important, this exercise highlighted the challenge of predicting weights between sparse reference data points, i.e., evaluating model uncertainty in a spatially continuous manner (Lu et al., 2024). While not demonstrated in this manuscript, we believe that the BMA offers a promising approach to tackle this issue, potentially facilitating a major shift from the "analysis" presented here to "synthesis" — combining different models spatially continuously as their estimated uncertainties evolve. One of the avenues we have explored, which certainly merits further attention, is how to stratify the local weights obtained from the "training plots" (80% of the data in the 5-fold cross-validation) for application to the "test plots" (remaining 20% of the data). Namely, as elaborated by Zhou (2012), under the stated gaussian assumption, the weighted sum presented in Eq. 4, i.e., without any stratification, does not necessarily provide a better fit to the reference data than any individual model.

We have explored several possible avenues for addressing this issue, such as stratifying based on the proximity of estimated height distributions among models or considering the forest ownership criterion. Additionally, we have examined potential modifications to the employed method that could enhance predictive skills. However, the marginal improvements obtained were insufficient for inclusion in this work, which is currently focused on analysis rather than prediction (i.e., interpolation/extrapolation). Instead, the avenues discussed serve as a foundation for future research, which could tackle the broader issue of spatial uncertainty evaluation. Another perspective for future work, and a more straightforward solution to this issue, would be to utilize a spatially continuous reference, such as the Lidar HD-derived canopy height map (Institut national de l'information géographique et forestière, 2024b) - once it becomes available for the entire area of interest. This approach would enable the automatic synthesis of spatialized mixtures. However, it is crucial to acknowledge that such reference height maps will not be entirely flawless due to various sources of heterogeneity, such as differences in sensors and acquisition seasons. As a result, they will need to be thoroughly processed before being considered as reliable as the NFI field measurements used in this study.

As for the methodological decision mentioned in Sec. 4.1 not to include the updated weights in the convergence as suggested by Raftery et al. (2003), we also tested the opposite approach, which is more common in the literature. However, this did not improve the goodness-of-fit shown in Fig. 5, but only increased the contrast between the local weights of individual models, favoring the overall dominant model. Therefore, we chose to present an analysis that yields at least equally effective higher-order mixtures while emphasizing the potential contributions of models that are not overall dominant.

It is important to note that limiting this study to France may lead to an overly optimistic evaluation of the models and their combinations. This is likely due to the availability of higher-quality training data in Europe compared to e.g. most tropical regions (e.g., fewer clouds, superior ALS data, and clearer topographic visibility in less dense forests) and boreal regions where no GEDI data is available. Additionally, the range of forest types, while extensive by European standards, is narrower compared to tropical forests, which are also characterized by denser stands and greater biomass. Consequently, remote sensing-

based forest attribute mapping faces significant challenges in tropical forests, which are not adequately addressed in this study focused on temperate European forests.

7 Conclusions

In this study we jointly interpreted the performances of five different remote sensing and AI based models for the high resolution mapping of the forest canopy height by combining them using the Bayesian model averaging framework and NFI in situ measurements. We observed that the participation of the different models varies depending on the height reference employed - maximum, mean, dominant or Lorey's, which can be directly linked to the different remote sensing input data. We also observed significant spatial variations in terms of the local weights, indicating that any attempt at model fusion should be tailored to the scale. A much more pronounced spread (comparable weights but contrasted predictions) of the analyzed models was observed in the regions with a pronounced topography, clearly indicating that the real challenge, at least in the temperate regions, is to do better in the mountains, by means of a better remote sensing data correction as well as a better modeling. The observed spread is also significantly impacted by the dominant tree species observed, the forest stand vertical structure, and the forest ownership type, the last-mentioned being a very good proxy for the forest stand complexity. The latter suggests that including these as modalities when possible could potentially improve the performances of the analyzed models. Nevertheless, the spread observed when using the BMA remained inferior to the within-variance, which was not the case when relying on the simple model average. All this suggests that the response to the paraphrased George Box's aphorism posed in the title — "some models are useful, but might they provide us with even more insights when combined?" — could indeed be affirmative in our context, particularly when employing BMA. However, it is important to note that these models should be complemented by a bias correction method, which is not addressed by the BMA methodology employed. Accordingly, it also failed to correct for the saturation of predicted height observed in individual models. It is also important to note that the BMA method we applied must be complemented by an appropriate stratification strategy before enabling the prediction, i.e. the fitting of spatially continuous higher-order mixture models, when using sparse reference data. In other words, such a strategy is necessary for estimating uncertainty between the *in situ* measurement points.

From an analytical standpoint, the most apparent direction for the presented work would be to move towards establishing a well-defined framework for evaluating models, possibly incorporating a denser network of references using GEDI measurements. The advantage of using the GEDI measurements would be the possibility to more easily relate the evaluated differences to the employed AI method or the choice of the complementary non-lidar measurements. Another perspective, particularly applicable when relying on GEDI measurements, would involve adapting the method for evaluating tree cover maps. This adaptation would necessitate a change in the probability distribution assumption (Eq. 2) from Gaussian to Bernoulli.

From a synthesis standpoint, the most compelling perspective of the presented work would be the ability to use the obtained local weights to effectively produce four finite spatialized mixtures, corresponding to dominant height, mean height, maximum height, and Lorey's mean height. This approach should facilitate the creation of an ensemble model for allometric wood volume or aboveground biomass (AGB) estimation. However, it necessitates either the availability of spatially continuous reference

data (Lidar HD data) or further methodological research at least partially focused the stratification of sparsely distributed local weights.

Code and data availability. The datasets corresponding to the five employed models are publicly available:

- M_1: https://doi.org/10.3929/ethz-b-000609802
- M_2: https://zenodo.org/records/8154445
- M_3: https://zenodo.org/records/8071004
- M_4: https://glad.umd.edu/dataset/gedi/
- M_5: https://zenodo.org/records/7840108

The python code used in the study, organized into three .py scripts and allowing the reproduction of the presented results, is available without restrictions at https://zenodo.org/records/11209336.

Due to legal restrictions (statistical confidentiality), the exact locations of the reference NFI plots used in the study cannot be disclosed. Therefore, the file (denoted as *Input_data_table.csv* in the provided code) containing extracts from the five employed models at the reference NFI plots, along with the NFI plots variables such as the four variants of reference height and other variables used in the study, is not directly available. However, a confidential access could be provided for the editor and reviewers if necessary to enable peer review.

Links for downloading all the other auxiliary datasets used in the study, such as the contours of French sylvo-ecological regions, are provided in the code.

Appendix A: Forest canopy height maps

This appendix contains figures which supplement Sections 2, 5 and 6.

Appendix B: Descriptive statistics

This appendix contains a figure which supplements Sec. 5.4.

Author contributions. NB conceived and carried out the study, interpreted the results and wrote the manuscript. NP, CV, PC and JDB contributed in establishing the methodological framework, supported the data preparation and helped the results interpretation. LH, JPR, GD and FM assisted in ameliorating the methodological framework. APT, FF, MS and MP helped the results interpretation.

Competing interests. The authors declare that they have no conflict of interest.
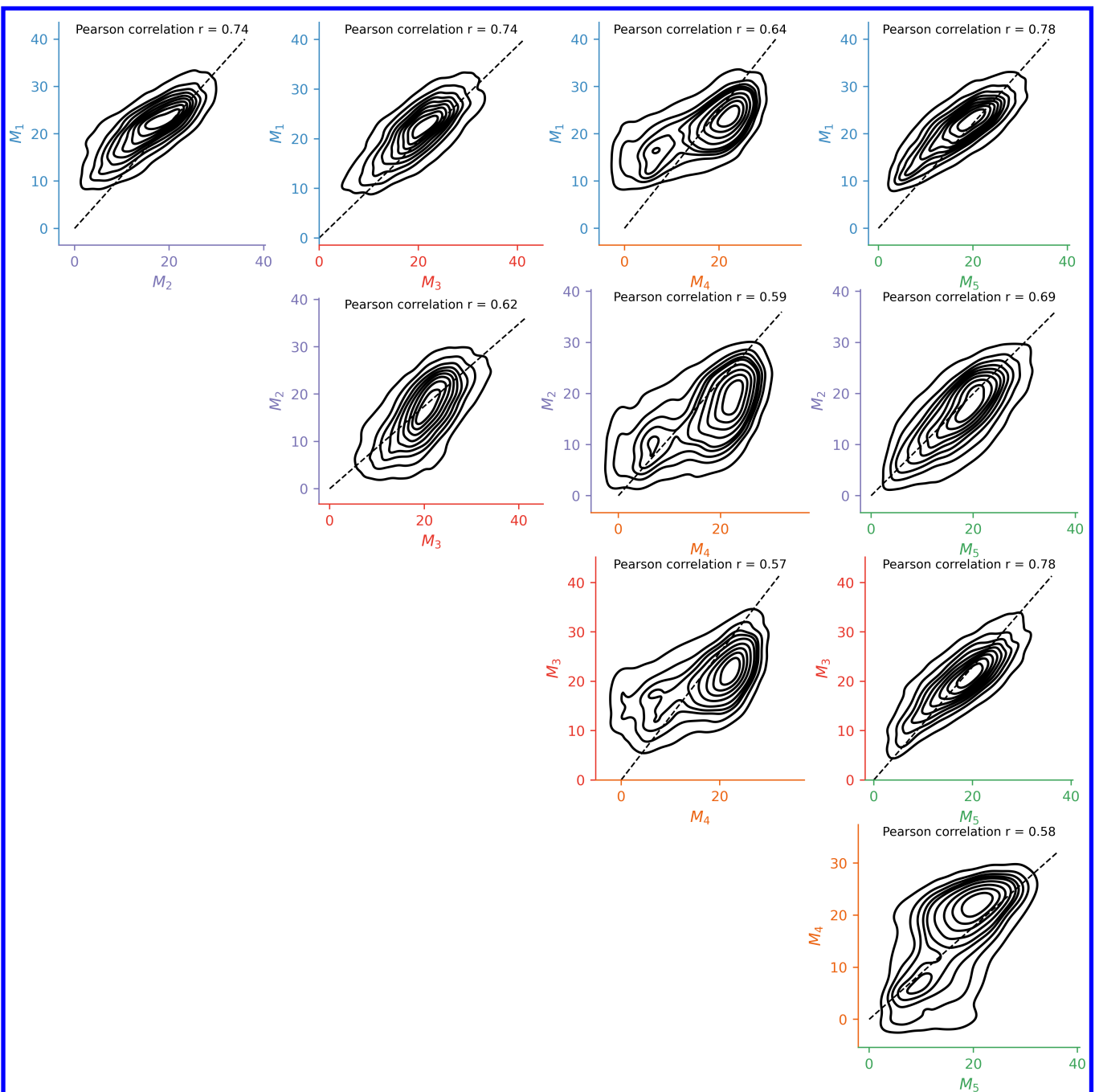
Figure A1. Kernel density estimate (KDE) plots mutually comparing individual models.
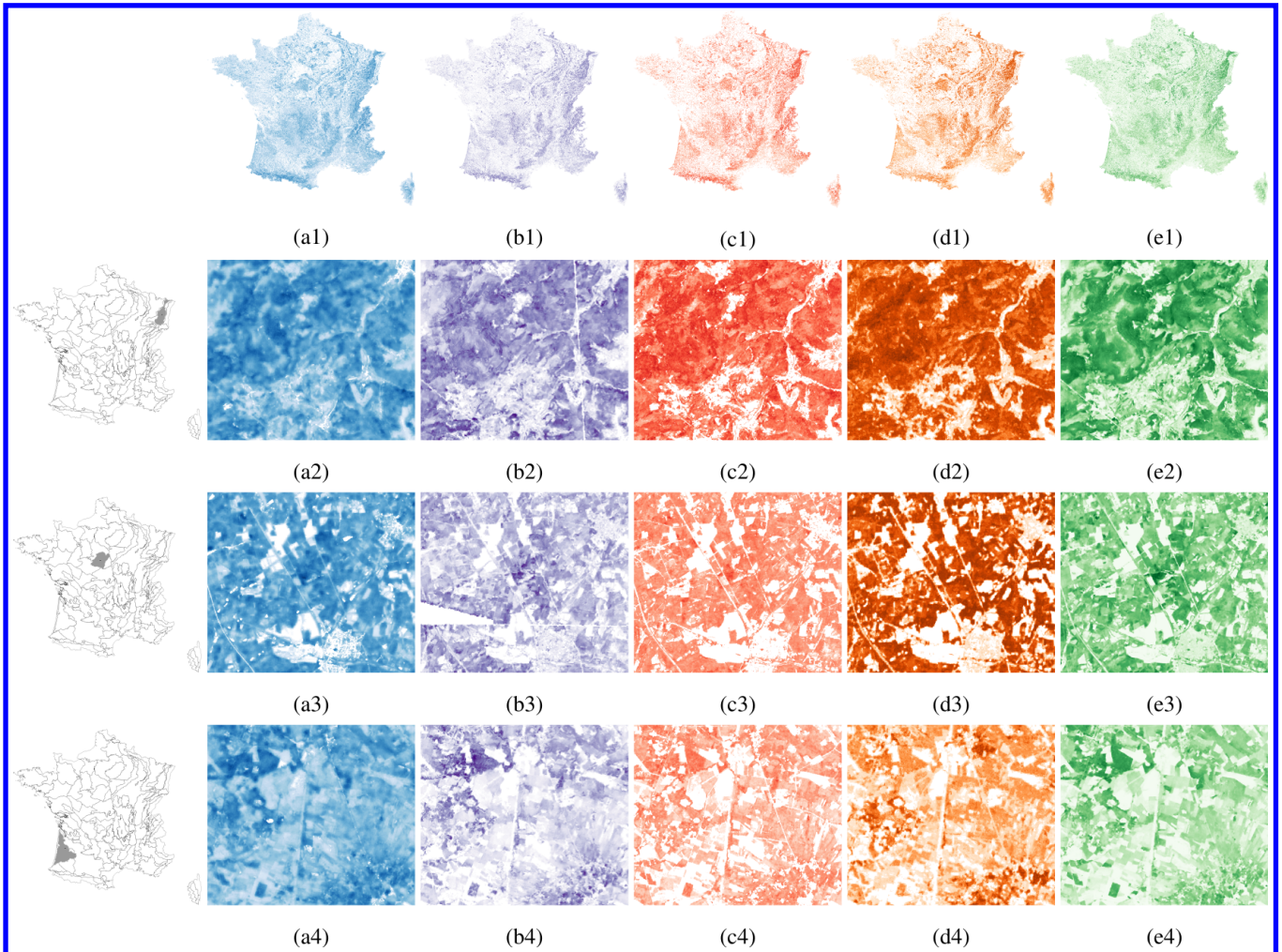
Figure A2. Forest canopy height maps produced by: (a) M_1 (Lang), (b) M_2 (Liu), (c) M_3 (Morin), (d) M_4 (Potapov), and (e) M_5 (Schwartz), illustrated for: (1) metropolitan France, (2) a zone in the Vosges Mountains, (3) a zone in Sologne Forest, and (4) a zone in the Landes de Gascogne. The leftmost column indicates the location of the highlighted zones within metropolitan France.
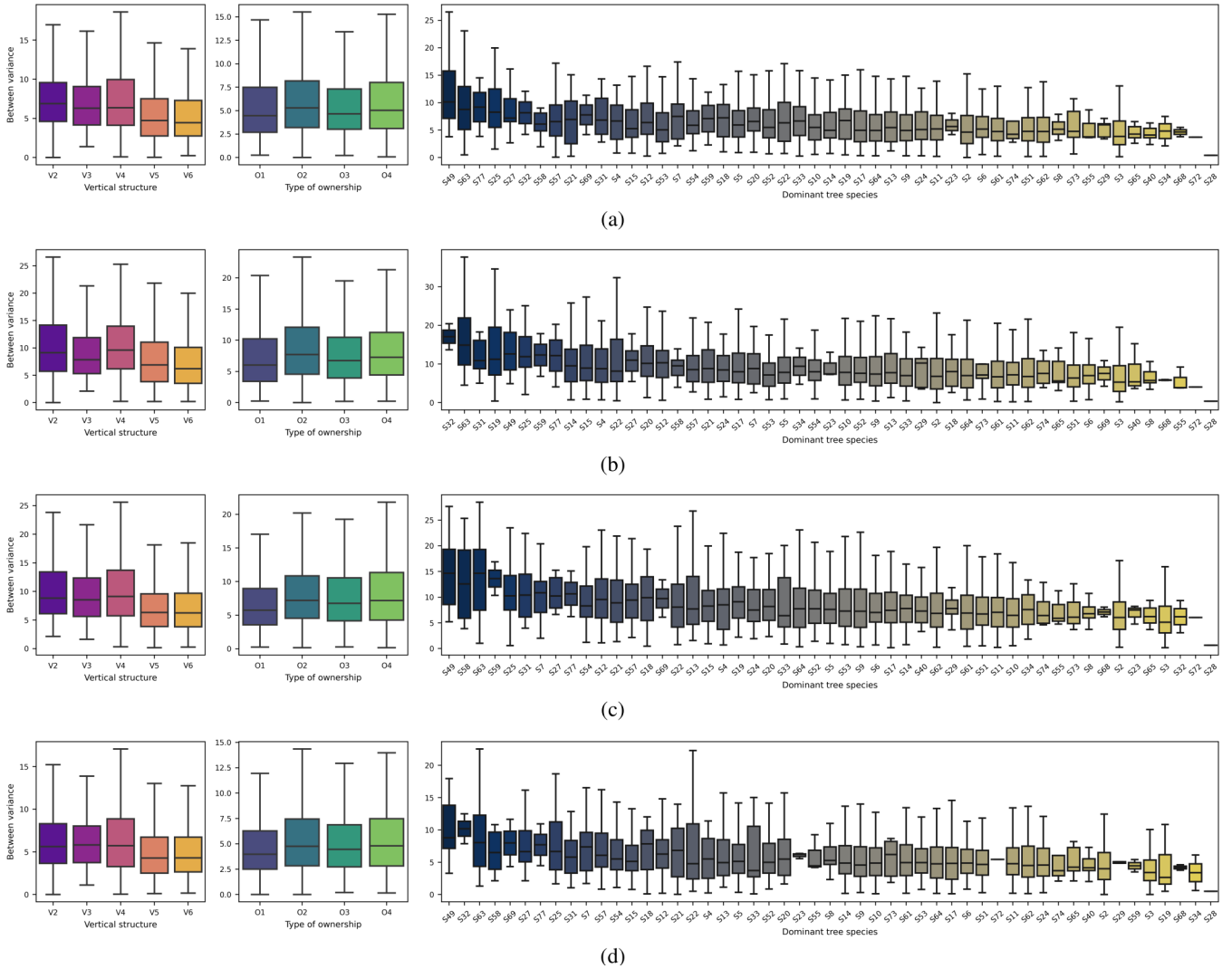
Figure B1. Boxplots illustrating the descriptive statistics of between variance for different levels of categorical variables, which have been shown to be statistically significant in terms of their influence on model spread, include the vertical structure (V), the type of forest ownership (O), and the dominant tree species (S). These are presented with references: (a) H_{dom}^i, (b) H_{mean}^i, (c) H_{max}^i, and (d) H_{lor}^i. V2 - regular low forest, V3 - other regular low stands, V4 - irregular vertical structure, V5 - regular high with understorey, V6 - regular high without understorey. O1 - managed private forest, O2 - unmanaged private forest, O3 - national (public) forest, O4 - any other public forest. S2 - *Quercus pedunculata*, S3 - *Quercus sessiliflora*, S4 - *Quercus rubra*, S5 - *Quercus lanuginosa*, S6 - *Quercus ilex*, S7 - *Quercus toza*, S8 - *Quercus suber*, S9 - *Fagus sylvatica*, S10 - *Castanea sativa*, S11 - *Carpinus betulus*, S12 - *Betula pubescens*, S13 - *Alnus glutinosa*, S14 - *Robinia pseudoacacia*, S15 - *Acer pseudoplatanus*, S17 - *Fraxinus excelsior*, S18 - *Ulmus campestris*, S19 - *Populus deltoides*, S20 - *Tilia cordata*, S21 - *Acer campestre*, S22 - *Prunus avium*, S23 - diverse fruit trees, S24 - *Populus tremula*, S25 - *Salix*, S27 - *Juglans regia*, S28 - *Olea europea*, S29 - other exotic broad-leaved, S31 - *Corylus avellana*, S32 - *Ostrya carpinifolia*, S33 - *Populus alba*, S34 - *Quercus cerris*, S40 - *Arbutus unedo*, S49 - other native broad-leaved, S51 - *Pinus pinaster*, S52 - *Pinus sylvestris*, S53 - *Pinus salzmannii*, S54 - *Pinus nigra*, S55 - *Pinus pinea*, S57 - *Pinus halepensis*, S58 - *Pinus uncinata*, S59 - *Pinus cembra*, S61 - *Abies alba*, S62 - *Picea abies*, S63 - *Larix decidua*, S64 - *Pseudotsuga menziesii*, S65 - *Cedrus atlantica*, S68 - other exotic coniferous, S69 - *Juniperus thurifera*, S72 - *Abies grandis*, S73 - *Picea sitchensis*, S74 - *Larix leptolepis*, S77 - *Pinus taeda*.

515 *Acknowledgements.* This research was partly supported by the ANR funded research project AI4Forest (ANR-22-FAI1-0002), as well as the PEPR Forestt PC Monitor research program.

We would like to thank the two anonymous reviewers, whose valuable feedback greatly contributed to improving the manuscript, particularly in identifying the limitations of the presented work, which opens up exciting research perspectives. We would as well like to thank IGN colleagues who collected, processed and organized the NFI field data. We would also like to thank the authors of the five employed models

520 for their outstanding work and in particular for sharing publicly the outputs of their models.

The English wording refinement was partly carried out using the publicly available GenAI (ChatGPT).

References

Bao, L., Gneiting, T., Grimit, E. P., Guttorp, P., and Raftery, A. E.: Bias Correction and Bayesian Model Averaging for Ensemble Forecasts of Surface Wind Direction, Monthly Weather Review, 138, 1811 – 1821, https://doi.org/10.1175/2009MWR3138.1, 2010.

Besic, N., Durrieu, S., Schleich, A., and Vega, C.: Using Structural Class Pairing to Address the Spatial Mismatch Between GEDI Measurements and NFI Plots, IEEE Journal of Selected Topics in Applied Earth Observations and Remote Sensing, 17, 12 854–12 867, https://doi.org/10.1109/JSTARS.2024.3425431, 2024a.

Besic, N., Picard, N., Sainte-Marie, J., Meliho, M., Piedallu, C., and Legay, M.: A Novel Framework and a New Score for the Comparative Analysis of Forest Models Accounting for the Impact of Climate Change, Journal of Agricultural, Biological and Environmental Statistics, 29, 73–91, https://doi.org/10.1007/s13253-023-00557-y, 2024b.

Bontemps, J.-D., Bouriaud, O., Vega, C., and Bouriaud, L.: Offering the appetite for the monitoring of European forests a diversified diet, Annals of Forest Science, 79, 19, https://doi.org/10.1186/s13595-022-01139-7, 2022.

Breiman, L.: Bagging predictors, Machine Learning, 24, 123–140, https://doi.org/10.1007/BF00058655, 1996.

Brigot, G., Simard, M., Colin-Koeniguer, E., and Boulch, A.: Retrieval of Forest Vertical Structure from PolInSAR Data by Machine Learning Using LIDAR-Derived Features, Remote Sensing, 11, https://doi.org/10.3390/rs11040381, 2019.

Coops, N. C., Tompalski, P., Goodbody, T. R. H., Queinnec, M., Luther, J. E., Bolton, D. K., White, J. C. Wulder, M. A., van Lier, O. R., and Hermosilla, T.: Modelling lidar-derived estimates of forest attributes over space and time: A review of approaches and future trends, Remote Sensing of Environment, 260, 112 477, https://doi.org/10.1016/j.rse.2021.112477, 2021.

Dempster, A. P., Laird, N. M., and Rubin, D. B.: Maximum Likelihood from Incomplete Data Via the EM Algorithm, Journal of the Royal Statistical Society: Series B (Methodological), 39, 1–22, https://doi.org/10.1111/j.2517-6161.1977.tb01600.x, 1977.

Dormann, C. F., Calabrese, J. M., Guillera-Arroita, G., Matechou, E., Bahn, V., Bartoń, K., Beale, C. M., Ciuti, S., Elith, J., Gerstner, K., Guelat, J., Keil, P., Lahoz-Monfort, J. J., Pollock, L. J., Reineking, B., Roberts, D. R., Schröder, B., Thuiller, W., Warton, D. I., Wintle, B. A., Wood, S. N., Wüest, R. O., and Hartig, F.: Model averaging in ecology: a review of Bayesian, information-theoretic, and tactical approaches for predictive inference, Ecological Monographs, 88, 485–504, https://doi.org/10.1002/ecm.1309, 2018.

Dubayah, R., Blair, J. B., Goetz, S., Fatoyinbo, L., Hansen, M., Healey, S., Hofton, M., Hurtt, G., Kellner, J., Luthcke, S., Armston, J., Tang, H., Duncanson, L., Hancock, S., Jantz, P., Marselis, S., Patterson, P. L., Qi, W., and Silva, C.: The Global Ecosystem Dynamics Investigation: High-resolution laser ranging of the Earth's forests and topography, Science of Remote Sensing, 1, 100 002, https://doi.org/10.1016/j.srs.2020.100002, 2020.

Duplat, P. and Perrotte, G.: Inventaire et estimation de l'accroissement des peuplements forestiers, Office national des forêts (ONF) - Section technique, Fontainebleau [France], ISBN 978-2-904384-00-4, 1982.

Ehbrecht, M., Schall, P., Ammer, C., and Seidel, D.: Quantifying stand structural complexity and its relationship with forest management, tree species diversity and microclimate, Agricultural and Forest Meteorology, 242, 1–9, https://doi.org/10.1016/j.agrformet.2017.04.012, 2017.

Erickson, M. J., Colle, B. A., and Charney, J. J.: Impact of Bias-Correction Type and Conditional Training on Bayesian Model Averaging over the Northeast United States, Weather and Forecasting, 27, 1449 – 1469, https://doi.org/10.1175/WAF-D-11-00149.1, 2012.

Evans, D. L., Roberts, S. D., and Parker, R. C.: LiDAR - A new tool for forest measurements?, The Forestry Chronicle, 82, 211–218, https://doi.org/10.5558/tfc82211-2, 2006.

Fassnacht, F. E., White, J. C., Wulder, M. A., and Næsset, E.: Remote sensing in forestry: current challenges, considerations and directions, Forestry: An International Journal of Forest Research, 97, 11–37, https://doi.org/10.1093/forestry/cpad024, 2023.

560 Fayad, I., Baghdadi, N., Alcarde Alvares, C., Stape, J. L., Bailly, J. S., Scolforo, H. F., Cegatta, I. R., Zribi, M., and Le Maire, G.: Terrain Slope Effect on Forest Height and Wood Volume Estimation from GEDI Data, Remote Sensing, 13, https://doi.org/10.3390/rs13112136, 2021.

Fayad, I., Ciais, P., Schwartz, M., Wigneron, J.-P., Baghdadi, N., de Truchis, A., d'Aspremont, A., Frappart, F., Saatchi, S., Sean, E., Pellissier-Tanon, A., and Bazzi, H.: Hy-TeC: a hybrid vision transformer model for high-resolution and large-scale mapping of canopy height, 565 Remote Sensing of Environment, 302, 113 945, https://doi.org/10.1016/j.rse.2023.113945, 2024.

Fogel, F., Perron, Y., Besic, N., Saint-André, L., Pellissier-Tanon, A., Schwartz, M., Boudras, T., Fayad, I., d'Aspremont, A., Landrieu, L., and Ciais, P.: Open-Canopy: A Country-Scale Benchmark for Canopy Height Estimation at Very High Resolution, https://arxiv.org/abs/2407.09392, 2024.

Ge, S., Gu, H., Su, W., Praks, J., and Antropov, O.: Improved Semisupervised UNet Deep Learning Model for Forest Height Mapping With 570 Satellite SAR and Optical Data, IEEE Journal of Selected Topics in Applied Earth Observations and Remote Sensing, 15, 5776–5787, https://doi.org/10.1109/JSTARS.2022.3188201, 2022.

Gibbons, J. M., Cox, G. M., Wood, A. T. A., Craigon, J., Ramsden, S. J., Tarsitano, D., and Crout, N. M. J.: Applying Bayesian Model Averaging to mechanistic models: An example and comparison of methods, Environmental Modelling & Software, 23, 973–985, https://doi.org/10.1016/j.envsoft.2007.11.008, 2008.

575 Hawes, A. F.: Conversion of Coppice Under Standards to High Forests in Eastern France, Journal of Forestry, 6, 151–157, https://doi.org/10.1093/jof/6.2.151, 1908.

Hervé, J.-C., Wurpillot, S., Vidal, C., and Roman-Amat, B.: L'inventaire des ressources forestières en France : un nouveau regard sur de nouvelles forêts, Revue forestière française, 66, 247 – 260, https://doi.org/10.4267/2042/56055, 2014.

Hoeting, J. A., Madigan, D., Raftery, A. E., and Volinsky, C. T.: Bayesian Model Averaging: A Tutorial, Statistical Science, 14, 382–401, 580 1999.

Hu, X., Madden, L. V., Edwards, S., and Xu, X.: Combining Models is More Likely to Give Better Predictions than Single Models, Phytopathology®, 105, 1174–1182, https://doi.org/10.1094/PHYTO-11-14-0315-R, 2015.

Imhoff, M. L.: A theoretical analysis of the effect of forest structure on synthetic aperture radar backscatter and the remote sensing of biomass, IEEE Transactions on Geoscience and Remote Sensing, 33, 341–351, https://doi.org/10.1109/TGRS.1995.8746015, 1995.

585 Institut national de l'information géographique et forestière: BD Alti, https://geoservices.ign.fr/bdalti, 2024a.

Institut national de l'information géographique et forestière: Lidar HD, https://geoservices.ign.fr/lidarhd, 2024b.

IPCC: Climate Change 2021: The Physical Science Basis. Contribution of Working Group I to the Sixth Assessment Report of the Intergovernmental Panel on Climate Change, vol. In Press, Cambridge University Press, Cambridge, United Kingdom and New York, NY, USA, 2021.

590 Irulappa-Pillai-Vijayakumar, D. B., Renaud, J.-P., Morneau, F., McRoberts, R. E., and Vega, C.: Increasing Precision for French Forest Inventory Estimates using the k-NN Technique with Optical and Photogrammetric Data and Model-Assisted Estimators, Remote Sensing, 11, https://doi.org/10.3390/rs11080991, 2019.

Joshi, N., Mitchard, E. T. A., Brolly, M., Schumacher, J., Fernández-Landa, A., Johannsen, V. K., Marchamalo, M., and Fensholt, R.: Understanding 'saturation' of radar signals over forests, Scientific Reports, 7, 3505, https://doi.org/10.1038/s41598-017-03469-3, 2017.

595 Kaufmann, J. and Schering, A.: Analysis of Variance ANOVA, John Wiley & Sons, Ltd, ISBN 9781118445112, https://doi.org/10.1002/9781118445112.stat06938, 2014.

Lang, N., Schindler, K., and Wegner, J. D.: Country-wide high-resolution vegetation height mapping with Sentinel-2, Remote Sensing of Environment, 233, 111 347, https://doi.org/10.1016/j.rse.2019.111347, 2019.

Lang, N., Jetz, W., Schindler, K., and Wegner, J. D.: A high-resolution canopy height model of the Earth, Nature Ecology & Evolution, 7, 600 1778–1789, https://doi.org/10.1038/s41559-023-02206-6, 2023.

Li, J., Hong, D., Gao, L., Yao, J., Zheng, K., Zhang, B., and Chanussot, J.: Deep learning in multimodal remote sensing data fusion: A comprehensive review, International Journal of Applied Earth Observation and Geoinformation, 112, 102 926, https://doi.org/10.1016/j.jag.2022.102926, 2022.

Li, Y., Andersen, H.-E., and McGaughey, R.: A Comparison of Statistical Methods for Estimating Forest Biomass from Light Detection and 605 Ranging Data, Western Journal of Applied Forestry, 23, 223–231, https://doi.org/10.1093/wjaf/23.4.223, 2008.

Liu, S., Brandt, M., Nord-Larsen, T., Chave, J., Reiner, F., Lang, N., Tong, X., Ciais, P., Igel, C., Pascual, A., Guerra-Hernandez, J., Li, S., Mugabowindekwe, M., Saatchi, S., Yue, Y., Chen, Z., and Fensholt, R.: The overlooked contribution of trees outside forests to tree cover and woody biomass across Europe, Science Advances, 9, eadh4097, https://doi.org/10.1126/sciadv.adh4097, 2023.

Lu, K., Bates, S., and Wang, S.: Quantifying uncertainty in area and regression coefficient estimation from remote sensing maps, https: 610 //arxiv.org/abs/2407.13659, 2024.

McLachlan, G. J. and Krishnan, T.: The EM algorithm and extensions, Wiley series in probability and statistics, Wiley-Interscience, Hoboken (N. J.), 2nd edition edn., ISBN 978-0-471-20170-0, 2008.

Meyer, H. and Pebesma, E.: Machine learning-based global maps of ecological variables and the challenge of assessing them, Nature Communications, 13, 2208, https://doi.org/10.1038/s41467-022-29838-9, 2022.

615 Mo, L., Zohner, C. M., Reich, P. B., Liang, J., de Miguel, S., Nabuurs, G.-J., Renner, S. S., van den Hoogen, J., Araza, A., Herold, M., Mirzagholi, L., Ma, H., Averill, C., Phillips, O. L., Gamarra, J. G. P., Hordijk, I., Routh, D., Abegg, M., Adou Yao, Y. C., Alberti, G., Almeyda Zambrano, A. M., Alvarado, B. V., Alvarez-Dávila, E., Alvarez-Loayza, P., Alves, L. F., Amaral, I., Ammer, C., Antón-Fernández, C., Araujo-Murakami, A., Arroyo, L., Avitabile, V., Aymard, G. A., Baker, T. R., Bałazy, R., Banki, O., Barroso, J. G., Bastian, M. L., Bastin, J.-F., Birigazzi, L., Birnbaum, P., Bitariho, R., Boeckx, P., Bongers, F., Bouriaud, O., Brancalion, P. H. S., Brandl, 620 S., Brearley, F. Q., Brienen, R., Broadbent, E. N., Bruelheide, H., Bussotti, F., Cazzolla Gatti, R., César, R. G., Cesljar, G., Chazdon, R. L., Chen, H. Y. H., Chisholm, C., Cho, H., Cienciala, E., Clark, C., Clark, D., Colletta, G. D., Coomes, D. A., Cornejo Valverde, F., Corral-Rivas, J. J., Crim, P. M., Cumming, J. R., Dayanandan, S., de Gasper, A. L., Decuyper, M., Derroire, G., DeVries, B., Djordjevic, I., Dolezal, J., Dourdain, A., Engone Obiang, N. L., Enquist, B. J., Eyre, T. J., Fandohan, A. B., Fayle, T. M., Feldpausch, T. R., Ferreira, L. V., Finér, L., Fischer, M., Fletcher, C., Frizzera, L., Gianelle, D., Glick, H. B., Harris, D. J., Hector, A., Hemp, A., Hengeveld, G., 625 Hérault, B., Herbohn, J. L., Hillers, A., Honorio Coronado, E. N., Hui, C., Ibanez, T., Imai, N., Jagodziński, A. M., Jaroszewicz, B., Johannsen, V. K., Joly, C. A., Jucker, T., Jung, I., Karminov, V., Kartawinata, K., Kearsley, E., Kenfack, D., Kennard, D. K., Kepfer-Rojas, S., Keppel, G., Khan, M. L., Killeen, T. J., Kim, H. S., Kitayama, K., Köhl, M., Korjus, H., Kraxner, F., Kucher, D., Laarmann, D., Lang, M., Lu, H., Lukina, N. V., Maitner, B. S., Malhi, Y., Marcon, E., Marimon, B. S., Marimon-Junior, B. H., Marshall, A. R., Martin, E. H., Meave, J. A., Melo-Cruz, O., Mendoza, C., Mendoza-Polo, I., Miscicki, S., Merow, C., Monteagudo Mendoza, A., Moreno, V. S., Mukul, 630 S. A., Mundhenk, P., Nava-Miranda, M. G., Neill, D., Neldner, V. J., Nevenic, R. V., Ngugi, M. R., Niklaus, P. A., Oleksyn, J., Ontikov, P., Ortiz-Malavasi, E., Pan, Y., Paquette, A., Parada-Gutierrez, A., Parfenova, E. I., Park, M., Parren, M., Parthasarathy, N., Peri, P. L., Pfautsch, S., Picard, N., Piedade, M. T. F., Piotto, D., Pitman, N. C. A., Poulsen, A. D., Poulsen, J. R., Pretzsch, H., Ramirez Arevalo,

F., Restrepo-Correa, Z., Rodeghiero, M., Rolim, S. G., Roopsind, A., Rovero, F., Rutishauser, E., Saikia, P., Salas-Eljatib, C., Saner, P., Schall, P., Schelhaas, M.-J., Schepaschenko, D., Scherer-Lorenzen, M., Schmid, B., Schöngart, J., Searle, E. B., Seben, V., Serra-Diaz, J. M., Sheil, D., Shvidenko, A. Z., Silva-Espejo, J. E., Silveira, M., Singh, J., Sist, P., Slik, F., Sonké, B., Souza, A. F., Stereńczak, K. J., Svenning, J.-C., Svoboda, M., Swanepoel, B., Targhetta, N., Tchebakova, N., ter Steege, H., Thomas, R., Tikhonova, E., Umunay, P. M., Usoltsev, V. A., Valencia, R., Valladares, F., van der Plas, F., Van Do, T., van Nuland, M. E., Vasquez, R. M., Verbeeck, H., Viana, H., Vibrans, A. C., Vieira, S., von Gadow, K., Wang, H.-F., Watson, J. V., Werner, G. D. A., Wiser, S. K., Wittmann, F., Woell, H., Wortel, V., Zagt, R., Zawiła-Niedźwiecki, T., Zhang, C., Zhao, X., Zhou, M., Zhu, Z.-X., Zo-Bi, I. C., Gann, G. D., and Crowther, T. W.: Integrated global assessment of the natural forest carbon potential, Nature, 624, 92–101, https://doi.org/10.1038/s41586-023-06723-z, 2023.

Moreira, A., Prats-Iraola, P., Younis, M., Krieger, G., Hajnsek, I., and Papathanassiou, K. P.: A tutorial on synthetic aperture radar, IEEE Geoscience and Remote Sensing Magazine, 1, 6–43, https://doi.org/10.1109/MGRS.2013.2248301, 2013.

Morin, D., Planells, M., Baghdadi, N., Bouvet, A., Fayad, I., Le Toan, T., Mermoz, S., and Villard, L.: Improving Heterogeneous Forest Height Maps by Integrating GEDI-Based Forest Height Information in a Multi-Sensor Mapping Process, Remote Sensing, 14, https://doi.org/10.3390/rs14092079, 2022.

Morin, D., Planells, M., Mermoz, S., and Mouret, F.: Estimation of forest height and biomass from open-access multi-sensor satellite imagery and GEDI Lidar data: high-resolution maps of metropolitan France, https://arxiv.org/abs/2310.14662, 2023.

Mutanga, O., Masenyama, A., and Sibanda, M.: Spectral saturation in the remote sensing of high-density vegetation traits: A systematic review of progress, challenges, and prospects, ISPRS Journal of Photogrammetry and Remote Sensing, 198, 297–309, https://doi.org/10.1016/j.isprsjprs.2023.03.010, 2023.

Picard, N., Henry, M., Mortier, F., Trotta, C., and Saint-André, L.: Using Bayesian Model Averaging to Predict Tree Aboveground Biomass in Tropical Moist Forests, Forest Science, 58, 15–23, https://doi.org/10.5849/forsci.10-083, 2012.

Pinheiro, J. C. and Bates, D. M.: Mixed-Effects Models in S and S-Plus, Springer, New York, NY, ISBN 978-0-387-22747-4, https://doi.org/10.1007/b98882, 2000.

Ploton, P., Mortier, F., Réjou-Méchain, M., Barbier, N., Picard, N., Rossi, V., Dormann, C., Cornu, G., Viennois, G., Bayol, N., Lyapustin, A., Gourlet-Fleury, S., and Pélissier, R.: Spatial validation reveals poor predictive performance of large-scale ecological mapping models, Nature Communications, 11, 4540, https://doi.org/10.1038/s41467-020-18321-y, 2020.

Potapov, P., Hansen, M. C., Kommareddy, I., Kommareddy, A., Turubanova, S., Pickens, A., Adusei, B., Tyukavina, A., and Ying, Q.: Landsat Analysis Ready Data for Global Land Cover and Land Cover Change Mapping, Remote Sensing, 12, https://doi.org/10.3390/rs12030426, 2020.

Potapov, P., Li, X., Hernandez-Serna, A., Tyukavina, A., Hansen, M. C., Kommareddy, A., Pickens, A., Turubanova, S., Tang, H., Edibaldo Silva, C., Armston, J., Dubayah, R., Blair, J. B., and Hofton, M.: Mapping global forest canopy height through integration of GEDI and Landsat data, Remote Sensing of Environment, 253, 112 165, https://doi.org/10.1016/j.rse.2020.112165, 2021.

Quirós, E., Polo, M.-E., and Fragoso-Campón, L.: GEDI Elevation Accuracy Assessment: A Case Study of Southwest Spain, IEEE Journal of Selected Topics in Applied Earth Observations and Remote Sensing, 14, 5285–5299, https://doi.org/10.1109/JSTARS.2021.3080711, 2021.

Raftery, A. E.: Bayesian model selection in structural equation models, in: Testing structural equation models, edited by Bollen, K. A. and Log, J. S., pp. 163–180, 1993.

Raftery, A. E., Madigan, D., and Hoeting, J. A.: Bayesian Model Averaging for Linear Regression Models, Journal of the American Statistical Association, 92, 179–191, 1997.

Raftery, A. E., Balabdaoui, F., Gneiting, T., and Polakowski, M.: Using Bayesian Model Averaging to Calibrate Forecast Ensembles, Tech. rep., University of Washington, technical Report no. 440, 2003.

Raftery, A. E., Gneiting, T. Fadoua Balabdaoui, F., and Polakowski, M.: Using Bayesian Model Averaging to Calibrate Forecast Ensembles, Monthly Weather Review, 133, 1155 – 1174, https://doi.org/10.1175/MWR2906.1, 2005.

675 Renaud, J., Sagar, A., Barbillon, P., Bouriaud, O., Deleuze, C., and Vega, C.: Characterizing the calibration domain of remote sensing models using convex hulls, International Journal of Applied Earth Observation and Geoinformation, 112, 102 939, https://doi.org/https://doi.org/10.1016/j.jag.2022.102939, 2022.

Riano, D., Chuvieco, E., Salas, J., and Aguado, I.: Assessment of different topographic corrections in Landsat-TM data for mapping vegetation types, IEEE Transactions on Geoscience and Remote Sensing, 41, 1056–1061, https://doi.org/10.1109/TGRS.2003.811693, 2003.

680 Robert, N., Vidal, C., Colin, A., Hervé, J., Hamza, N., and Cluzeau, C.: French National Forest Inventory, in: National Forest Inventories, edited by Tomppo, E., Gschwantner, T., and Lawrence, M., chap. 12, Springer Netherlands, 2010.

Ronneberger, O., Fischer, P., and Brox, T.: U-Net: Convolutional Networks for Biomedical Image Segmentation, 2015.

Roy, D. P., Kashongwe, H. B., and Armston, J.: The impact of geolocation uncertainty on GEDI tropical forest canopy height estimation and change monitoring, Science of Remote Sensing, 4, 100 024, https://doi.org/10.1016/j.srs.2021.100024, 2021.

685 Schleich, A., Durrieu, S., Soma, M., and Vega, C.: Improving GEDI Footprint Geolocation Using a High-Resolution Digital Elevation Model, IEEE Journal of Selected Topics in Applied Earth Observations and Remote Sensing, 16, 7718–7732, https://doi.org/10.1109/JSTARS.2023.3298991, 2023.

Schwartz, M., Ciais, P., Ottlé, C., De Truchis, A., Vega, C., Fayad, I., Brandt, M., Fensholt, R., Baghdadi, N., Morneau, F., Morin, D., Guyon, D., Dayau, S., and Wigneron, J.-P.: High-resolution canopy height map in the Landes forest (France) based on GEDI, Sentinel-1, and

690 Sentinel-2 data with a deep learning approach, International Journal of Applied Earth Observation and Geoinformation, 128, 103 711, https://doi.org/10.1016/j.jag.2024.103711, 2024.

Stage, A. R. and Salas, C.: Interactions of Elevation, Aspect, and Slope in Models of Forest Species Composition and Productivity, Forest Science, 53, 486–492, https://doi.org/10.1093/forestscience/53.4.486, 2007.

Stekhoven, D. J. and Bühlmann, P.: MissForest Non-Parametric Missing Value Imputation for Mixed-Type Data, Bioinformatics, 28, 112–

695 118, https://doi.org/10.1093/bioinformatics/btr597, 2012.

Tan, M. and Le, Q. V.: EfficientNet: Rethinking Model Scaling for Convolutional Neural Networks, 2020.

Tang, H., Stoker, J., Luthcke, S., Armston, J., Lee, K., Blair, B., and Hofton, M.: Evaluating and mitigating the impact of systematic geolocation error on canopy height measurement performance of GEDI, Remote Sensing of Environment, 291, 113 571, https://doi.org/10.1016/j.rse.2023.113571, 2023.

700 Teillet, P., Guindon, B., and Goodenough, D.: On the Slope-Aspect Correction of Multispectral Scanner Data, Canadian Journal of Remote Sensing, 8, 84–106, https://doi.org/10.1080/07038992.1982.10855028, 1982.

Tolan, J., Yang, H.-I., Nosarzewski, B., Couairon, G., Vo, H. V., Brandt, J., Spore, J., Majumdar, S., Haziza, D., Vamaraju, J., Moutakanni, T., Bojanowski, P., Johns, T., White, B., Tiecke, T., and Couprie, C.: Very high resolution canopy height maps from RGB imagery using self-supervised vision transformer and convolutional decoder trained on aerial lidar, Remote Sensing of Environment, 300, 113 888,

705 https://doi.org/10.1016/j.rse.2023.113888, 2024.

Tomppo, E., Gschwantner, T., and Lawrence, M., eds.: National Forest Inventories, Springer Netherlands, 2010.

Tran-Ha, M., Cordonnier, T., Vallet, P., and Lombart, T.: Estimation of the total aerial volume of forest stands based on the basal arer and Lorey's height, Revue Forestiere Francaise, 63, 361–378, 2011.

Vanonckelen, S., Lhermitte, S., and Van Rompaey, A.: The effect of atmospheric and topographic correction methods on land cover classification accuracy, International Journal of Applied Earth Observation and Geoinformation, 24, 9–21, https://doi.org/https://doi.org/10.1016/j.jag.2013.02.003, 2013.

Wadoux, A. M.-C., Heuvelink, G. B., de Bruin, S., and Brus, D. J.: Spatial cross-validation is not the right way to evaluate map accuracy, Ecological Modelling, 457, 109 692, https://doi.org/10.1016/j.ecolmodel.2021.109692, 2021.

Wadoux, A. M. J.-C. and Heuvelink, G. B. M.: Uncertainty of spatial averages and totals of natural resource maps, Methods in Ecology and Evolution, 14, 1320–1332, https://doi.org/10.1111/2041-210X.14106, 2023.

Waser, L. T., Rüetschi, M., Psomas, A., Small, D., and Rehush, N.: Mapping dominant leaf type based on combined Sentinel-1/-2 data – Challenges for mountainous countries, ISPRS Journal of Photogrammetry and Remote Sensing, 180, 209–226, https://doi.org/10.1016/j.isprsjprs.2021.08.017, 2021.

Wintle, B. A., McCarthy, M. A., Volinsky, C. T., and Kavanagh, R. P.: The Use of Bayesian Model Averaging to Better Represent Uncertainty in Ecological Models, Conservation Biology, 17, 1579–1590, https://doi.org/10.1111/j.1523-1739.2003.00614.x, 2003.

Yang, X., Qiu, S., Zhu, Z., Rittenhouse, C., Riordan, D., and Cullerton, M.: Mapping understory plant communities in deciduous forests from Sentinel-2 time series, Remote Sensing of Environment, 293, 113 601, https://doi.org/10.1016/j.rse.2023.113601, 2023.

Yu, Q., Ryan, M. G., Ji, W., Prihodko, L., Anchang, J. Y., Kahiu, N., Nazir, A., Dai, J., and Hanan, N. P.: Assessing canopy height measurements from ICESat-2 and GEDI orbiting LiDAR across six different biomes with G-LiHT LiDAR, Environmental Research: Ecology, 3, 025 001, https://doi.org/10.1088/2752-664X/ad39f2, 2024.

Zhou, Z.-H.: Ensemble methods: foundations and algorithms, chap. 4.3.3, CRC press, 2012.